# NUMERICAL AND EXPERIMENTAL INVESTIGATION OF BLENDED WING BODY CONFIGURATION

*A Thesis*

*submitted in partial fulfilment of the requirements*

*for the award of the degree of*

**MASTER OF ENGINEERING**

**IN**

**SPACE ENGINEERING AND ROCKETRY**

**BY**

**MIDHUN MV**

**(ME/SER/10009/2017)**


**DEPARTMENT OF SPACE ENGINEERING AND ROCKETRY**

**BIRLA INSTITUTE OF TECHNOLOGY**

**MESRA - 835215, RANCHI**

**2019**

# DECLARATION

I certify that

a) The work contained in the thesis is original and has been done by myself under the general supervision of my supervisor.
b) The work has not been submitted to any other Institute for any degree or diploma.
c) I have followed the guidelines provided by the Institute in writing the thesis.
d) I have confirmed to the norms and guidelines given in the Ethical Code of Conduct of the Institute.
e) Whenever I have used materials (data, theoretical analysis, and text) from other sources, I have given due credit to them by citing them in the text of the thesis and giving their details in the references.
f) Whenever I have quoted written materials from other sources, I have put them under quotation marks and given due credit to the sources by citing them and giving required details in the references.

(Midhun MV)

Roll No.: ME/SER/10009/2017

# APPROVAL OF THE GUIDE

Recommended that the thesis entitled "**Numerical and Experimental Investigation of Blended Wing Body Configuration**" prepared by Mr. Midhun MV under my supervision and guidance be accepted as fulfilling this part of the requirements for the degree of Master of Engineering.

To the best of my knowledge, the contents of this thesis did not form a basis for the award of any previous degree to anyone else.

Date:

(DR. PARTHA MONDAL)
Assistant Professor
Department of Space Engineering and Rocketry
BIT, Mesra, Ranchi.

# THESIS APPROVAL CERTIFICATE

This is to certify that the work embodied in this thesis entitled "**NUMERICAL AND EXPERIMENTAL INVESTIGATION OF BLENDED WING BODY**" is carried out by Mr. Midhun MV (Roll No. ME/SER/10009/2017) is approved for the degree of Master of Engineering of Birla Institute of Technology; Mesra, Ranchi.

Date:

Place: BIT Mesra, Ranchi

**Internal Examiner(s)** **External Examiner(s)**

**Name & Signature** **Name & Signature**

**Chairman**

**(Head of the Department)**

# ACKNOWLEDGEMENT

It gives me immense pleasure to acknowledge all the people for contributing to make this thesis a success.

I wish to express my sincere gratitude to my guide Dr. Partha Mondal, Department of Space Engineering and Rocketry, for the moral support, continuous involvement, always being willing and ready to answer my questions. I wish to thank Prof. Sudip Das, Head, Department of Space Engineering and Rocketry for his support. I offer my sincere gratitude to my teachers Dr Mohan Verma, Dr Swarup Jejurkar, Dr Shelly Biswas, Dr Rajeev Kumar, and Dr Priyank Kumar for their valuable suggestions and wholehearted co-operation.

I also owe thanks to my juniors specially; I am very grateful to Avik Arora for his enthusiasm towards my project and his insightful questions and all his help over the course of my thesis.

I would also like to thank Pawan Kumar Karn and the other PhD scholars for sharing their expertise and support during the experiments.

To my friends: thank you for your friendship, support, encouragement and most importantly, the laughs, the breaks, and the memories and a special thanks to Nivetha for her countless help.

I wish to thank my beloved parents for their endless love, continuous encouragement and support throughout my career.

Date: MIDHUN MV

Place: BIT, Mesra, Ranchi (ME/SER/10009/17)

# ABSTRACT

With the increasing concern for the environment and the depleting fuels, research has been going on to develop a more efficient and environmentally friendly aircrafts, hence unconventional designs are gaining popularity in the recent decades. Blended Wing Body configuration has an unconventional design in which the wing and fuselage are blended to form an aircraft. Researches have shown that this design concept offers a significant improvement in the aerodynamic efficiency compared to the conventional aircraft yet the concept has to developed for the commercial transport aircrafts. The current study focuses on the aerodynamic characteristics of the blended wing body configuration at low subsonic speed. A 3-D blended wing body is designed and numerical and experimental analysis are carried to describes the flow behaviour over the model. Aerodynamic characteristics and flow features obtained from the CFD analysis have been studied, analysed and compared with the experimental results. The BWB model designed have shown satisfied results. The optimum cruise angle for this model was found to be 6º where maximum L/D ratio was achieved. The flow separation was observed over the wing at low angle of attack yet the whole body experienced stalled at an angle of attack of around 45º. The results obtained shows that the blended wing body configuration can operates at high angle of attack.

# CONTENTS

# NOMENCLATURE

| | |
|---|---|
| $\widetilde{\nu_T}$ | Modified Eddy Viscosity |
| $\tilde{\nu}$ | Kinematic Turbulent Eddy Viscosity |
| μ | Coefficient of viscosity |
| $A_1$, $A_2$ | Axial Forces |
| b | Total span of the model |
| c | Root chord |
| $C_A$ | Axial Force Coefficient |
| $C_D$ | Drag Coefficient |
| $C_L$ | Lift Coefficient |
| $C_N$ | Normal Force Coefficient |
| Cp | Static Pressure Coefficient |
| $M_\infty$ | Freestream Mach Number |
| $N_1$, $N_2$ | Normal Forces |
| $q_\infty$ | Dynamic pressure |
| Re | Reynolds Number |
| $S_{ref}$ | Reference area of the model |
| $U_\infty$ | Freestream velocity |
| x/c | Non-dimensional distance along the root chord |
| y/(b/2) | Non-dimensional distance along the half span of the model |
| $y^+$ | Non-dimensional distance from the wall |
| α | Angel of Attack |
| ν | Molecular Kinematic Viscosity |
| ρ | Density of air |

# ABBREVATIONS

| | |
|---|---|
| ABS | Acrylonitrile Butadiene Styrene |
| AoA | Angle of Attack |
| BWB | Blended Wing Body |
| CAD | Computer Aided Design |
| CFD | Computational Fluid Dynamics |
| DAQ | Data Acquisitions System |
| FFF | Fused Filament Fabrication |
| GAMBIT | Geometry and Mesh Building Intelligent Tool |
| GAMG | Geometric Algebraic Multi-grid |
| L/D Ratio | Lift to Drag Ratio |
| MOB | Multidisciplinary Optimization of Blended Wing Body |
| NACA | National Advisory Committee for Aeronautics |
| NASA | National Aeronautics and Space Administration |
| OpenFOAM | Open source Field Operation and Manipulation |
| RANS | Reynolds-averaged Navier Stokes |
| SA | Spalart-Allmaras |
| UAV | Unmanned Air Vehicle |
| VELA | Very Efficient Large Aircraft |
| VLM | Vortex Lattice Method |

# LIST OF FIGURES

Page No.

# LIST OF TABLES

Page No.

# CHAPTER 1

# INTRODUCTION

Ever since the first aircraft designed and flown by Wright Brothers in 1903, many improvements were done to achieve better design and performances. But much of the advancements were made in the aerodynamics, propulsion systems, structures, materials and electronics and apart from the minor changes, the blueprint of the airplane geometry i.e. the classic tube and wing design has always been constant. Hence to get a breakthrough in the performance of current aircrafts, unconventional methods like morphing configuration, innovative controls and unconventional designs has to be implemented. The unconventional aircraft designs such as Flying Wing, Hybrid Wing, and Blended Wing Body configurations etc. have shown potential which otherwise might be impossible to achieve.

## 1.1 BLENDED WING BODY (BWB)

The Blended-Wing-Body (BWB) configuration merges the fuselage with the wing and eliminates the tail. Since the wings blends smoothly into a wide flat tailless fuselage, this fuselage produces most of the lift. Studies have shown that the BWB configuration have the potential to reduce fuel burn significantly, hence reduced operating cost and have shown promising aerodynamic efficiency with the entire aircraft generating the lift with minimum drag, hence increasing the fuel economy and range[1].

The BWB concept has been inspired from the flying wing aircraft, it combined the advantages of flying wing with the loading capabilities of that of traditional aircraft, by increasing the volume of the wing at the center to act as a fuselage. This allows BWB aircraft to carry more passengers and cargos.

With the elimination of tail and transforming it into a single lifting body, the wetted area to volume ratio is also reduced and thereby has lower interference drag. The BWB configuration also offers environmental and some unique safety advantages. By placing the engines above the wing, the engine noise will not be interacting with the wing’s lower surface, hence has a low acoustic signature.

Despite the numerous advantages of the BWB configuration, certain challenges exist. For instance, due to the elimination of tail and an unconventional shape, one of the critical aspects of the BWB is its control and stability. Designing and allocation of the control surfaces is crucial. Also, since the BWB is a blend of fuselage and wing, specifying a center body structure becomes a challenge. As a result, several studies have been done to carefully design and optimize the fuselage section in order to fulfill both the aerodynamic and structural analysis.

## 1.2 PREVIOUS MAJOR PROJECTS

Flying wing is not a new concept and have been of interest for more than a half century now. The world's first jet-powered flying wing aircraft, Horten Ho-229, was designed in 1940s during the World War II in Germany by the Horton brothers. Ever since then, several research groups, organizations are working continuously to produce an aerodynamically efficient aircrafts which has an advantage over the conventional aircraft designs.

### 1.2.1 NASA and the Boeing Company, USA

The NASA sponsored project includes Boeing, NASA Lewis, NASA Langley, University of Florida, Stanford University, Clark-Atlanta University, and University of Southern California all working to demonstrate the feasibility of the Blended Wing concept. The first BWB aircraft was conceptualized in 1988 by Robert to design a subsonic commercial aircraft capable of carrying 800 passengers, with 7000-nautical-mile design range at Mach 0.85[1,2,4]. When compared with a conventional airplane for a 7000-nautical-mile range, it was been found that, the BWB aircraft burned 27% lower fuel, had 15% lower take-off weight, 27% lower total thrust, and a 20% higher lift/drag ratio. These significant advantages of BWB over conventional aircraft are due to BWB configuration itself rather than some specifics improvements in aerodynamics or structures.

The potential of BWB concept was recognised and considered as a revolutionary design and ever since then the interest in BWB configuration continued to grow over the years. Hence Boeing started a preliminary design study of BWB transport in 2003 with advanced research, design methods and multi-disciplinary technology. A Boeing BWB-450 baseline Airplane was designed and compared with the existing aircrafts A380, B747, and A340.For optimization of shape and

configuration, Boeing developed an indigenous multidisciplinary airplane design optimization code called WingMOD. Besides aerodynamics and propulsion, structural analysis was also considered as a design parameter and played a key role in BWB design. Liebeck has discussed the unique opportunities and challenges in more detail[4].

### 1.2.2 MOB Project, Europe

MOB project[7] was a collaborative project between research institutes, universities and companies across Europe whose main goal was study the aerodynamics, structural, aeroelastic and flight mechanics of BWB at different levels. The baseline BWB geometry was designed with total span of less than 80m including the winglets and with no power plant section. Due to the tailless design concept, the stability and control issues were considered critical during the design process. A multi-level, multidisciplinary design tool, Computation Design Engine (CDE) was developed and applied to the BWB aircraft.

Qin et al[7] has done an extensive study on the aerodynamics advantages and features of the BWB at Sheffield University. The key aspects were the reduced wave drag, effect of spanwise load distribution and 2-D and 3-D optimisation for performance improvement and with forward swept wings.

### 1.2.3 Very Efficient Large Aircraft (VELA) Project

Airbus along with 17 European partners from industry and research worked together to explore more about the BWB configuration as a part of VELA project. In this project, each configuration was defined by its two leading edge sweep angles on the outboard and inboard wing sections and different cabin geometry. Optimisation includes the 2-D aerofoil design optimisation, 3-D twist and chord-length optimisation and CFD analysis were performed. Additional works included the determination of static and dynamic derivatives for stability and handling, high speed testing and even the effects of engines were also studied. Winglets along with control surfaces were also studied to understand its effects on control derivatives.

Apart from few major projects mentioned above, several aircraft industries, research institutes and academia have been researching to explore more and study in greater depth about the challenges and opportunities presents in the BWB

configuration. This research has discovered a great deal of advantages and some challenges. and these concepts are summarized in the next section.

## 1.3 ADVANTAGES AND DISADVANTAGES OF THE BLENDED WING BODY

Most of the benefits of blended wing configuration comes from its large aerodynamic gain due to integration of wing with the fuselage.

- Aerodynamics:
    - Low wetted area to volume ratio.
    - Low interference drag.
- Structures:
    - Since the whole aircraft act as a single body, which results in reduced bending moment and thus has reduced structural weight.
    - Promising span loading.
- Manufacturing:
    - Economical due to the simplicity of the BWB configuration.
    - Larger volume compared to conventional aircrafts hence more payload as well as passengers.

Despite the promising advantages of the Blended wing configuration, there are certain challenges which exists:

- Difficulty in the smooth transition from the thicker center body aerofoils to the thinner outer wing aerofoils.
- Integration of propulsion systems and airframes will increase the complexity of the design of this region.
- Elimination of tail have a great impact on the performance and stability of the aircraft, hence difficult controllability and stability.
- Pressurizing the cabin in BWB is difficult as compared to that of the conventional configuration.

## 1.4 OpenFOAM

The OpenFOAM (Open Field Operation and Manipulation) CFD is a free, opensource software used to solve complex fluid flows[26]. The OpenFOAM can run incompressible, compressible and multiphase flows, flows involving turbulence, chemical reactions and heat transfer, solid mechanics, electromagnetics etc. OpenFOAM is gaining popularity in the both commercial and academic organisations in recent years. OpenFOAM is chosen instead of the other CFD packages because:

- Is open source- free software with source code available to adapt and build new functionalities.
- Can easily work in parallel.
- Increasing popularity in industries, R&D centres and universities.
- Is community driven with millions of users working on various fields of application.

Although there are many advantages of OpenFOAM available, it is still a relatively new CFD package. Program errors and bugs are still possible and often reported in the community. Therefore, more verification and validation are required.

## 1.5 OUTLINE OF THE THESIS

A brief outline of the main chapters of the thesis are as follows:

Chapter 2 discusses the relevant research papers and journals gone through during the project. Chapter 3 describes the methodologies and techniques used for the design and analysis of Blended Wing Body configuration. Chapter 4 presents and discusses the computational and experimental results obtained. Chapter 5 includes the main conclusions drawn from the results. Chapter 6 focuses on the future area of research in this field.

# CHAPTER 2

# LITERATURE SURVEY

## OUTLINE

A meticulous review of related research works is an essential criterion to define the scope of the present project. This section will provide an evaluative report of the information found in the literatures related to the blended wing body. The survey here defines the area focused to the aerodynamic analysis of BWB configurations proving it more efficient than the existing conventional configurations. The other relevant papers related to modelling, optimizations and stability analysis of BWB configurations are included to provide better understanding.

## 2.1 PRIOR RESEARCH WORKS

In the late 90s, Liebeck et al.[1] introduced the Blended Wing Body configuration as a subsonic commercial transport which offered great advantages in terms of performance over the conventional, transonic transports. The team studied the preliminary aerodynamics of the configuration using CFD and worked on designing a highly integrated and aerodynamically efficient configuration. The study was mainly focused on the aerodynamic aspects of the BWB wing.

Liebeck[2] compared an BWB with a conventional aircraft of same capacity for 800 passengers and range of 7000NM. The BWB was designed by transforming a 650$m^2$ ball into a cylinder and then streamlined it to accommodate 800 passengers. A conventional aircraft with 4 engines has a wetted surface area of 4100$m^2$ while the BWB configuration has only 2800$m^2$ for same passenger capacity. There was a 33% reduction in wetted surface area, due to which total drag reduces, and thus will have higher L/D ratio when compared to a conventional aircraft. Optimization techniques helped in further improving the performances[3]**.** There was a reduction in takeoff weight and fuel burn and an increase in L/D ratio. All of these benefits were due to the BWB configuration itself, rather than specific traditional technologies such as aerodynamics or structures. BWB configurations can cruise at Mach 0.95. Results proved the superior characteristics of the BWB concept beyond the expectations[4].

The issues of size and application, design cruise Mach number, and stability were discussed as design challenges for the BWB concept[3]**.** The global design challenge of the BWB was to design a common airframe for both the military and commercial aircraft which will also show better performance than that of the existing airplanes.

P Dehpanah[5] studied the aerodynamic aspects of different blended wing body airframe using computational analysis. The first BWB airframe was a simple scaled design and then based on the numerical analysis of this model, a modified full-scaled blended-wing-body configuration airframe was developed with space for 800 passengers for long-range missions. RANS approach with SA model was used for the simulating the first design. The aerodynamic characteristics, spanwise lift and cross-sectional area distribution were studied and based on the results, an improved second model was designed and again analysis was performed on that. This design approach claims to utilize the maximum aerodynamic properties for designing BWB configuration.

Zurriati Mohd Ali et al.[6] reported an improved stability in the BWB configuration by using a small horizontal stabilizer called as canard. CFD analysis were conducted to determine the aerodynamics characteristic ($C_L$, L/D and Cm) of BWB incorporated with the canard. They have reported an improved pitching moment when canard was deflected at higher angles ($\delta = 10°$) and concluded that these configurations can improve pitching moment of BWB.

N. Qin et al.[7] presented the aerodynamic study of blended wing body (BWB) configuration designed under the European project, MOB. A series of computational analysis were carried out for the baseline BWB configuration and the aerodynamic analysis were performed. A 2-D aerofoil optimisation were done to further improve the aerodynamic performance. This optimised aerofoil was then used in designing the BWB wing and was further investigated. They achieved a 20% increase in L/D through 2-D aerofoil optimisation compared with baseline configuration. To get the full 3-D effect, a 3-D optimisation was performed with different constraints and then aerodynamic analysis were done. It was found that the optimal spanwise lift distribution for best aerodynamic performance should be a fine balance of the vortex induced drag due to lift and the wave drag due to the shock wave formation at transonic speeds. The

study also reveals that for the BWB design the pressure drag is playing a much more important role in the total drag as compared with the conventional designs.

Roberto Merino-Martinez[8] designed a BWB aircraft baseline and studied its aerodynamic performance and the Euler-based shape optimisation were done considering its challenging stability and control features**.** They performed an iterative optimisation process to obtain the minimum size of the control surfaces minimum drag and satisfactory performance characteristics. Aerodynamic results obtained using Vortex Lattice Method (VLM) and 3-D panel method were in close agreement with each other. A global 12% reduction of the control surfaces area was achieved, which implies lower weight and drag.

D. Roman et. Al[9] developed a blended wing body (BWB) configuration to determine its feasibility at transonic speeds, from M=0.85 to M=0.93. the model was first analysed using CFD, which was then optimized in WingMOD. They concluded that Mach 0.93 is feasible but there is a decrease in performance compared to Mach 0.85 and further increases will results in substantial increase in the drag, hence making the model unfeasible. For the tested BWB model, Mach 0.90 is the optimum cruising speed, at which it offered an improved characteristic with minimal drag.

Zhoujie Lyu[10] performed shape optimisation and numerical analysis using RANS with SA model. The study also discussed about the different constrains and design variables to be considered on the blended-wing-body configurations and the benefits and effect on it on optimised BWB model. Trim and static stability analysis were also performed at different flight conditions. The concluded that the aerodynamic performance depends on the spanwise lift distribution. The lowest drag was obtained for an elliptical spanwise lift distribution. From the results of these studies, RANS-based shape optimization has been proven as a useful tool for practical aircraft designing, especially designing of unconventional aircraft like BWB configurations.

Okonkwo et al.[11,12] reviewed the evolving trends in the design and challenges faced during the designing of the BWB airplane and developed a multi-variate optimisation tool which was used for designing and analysing the BWB commercial transport aircraft.

N.B Kuntawala[13,14] presented the flow analysis and aerodynamic shape optimisation of the BWB configuration**.** The baseline geometry was designed for a Mach number of 0.85 with range and altitude of 6000NM and 41,000ft respectively. His design included dihedral, twist, and sweep in the outer wing which improved the stability and also stall was delayed. At cruise Mach 0.85, they observed a 38.7% reduction in the drag (induced drag and wave drag) was achieved at the target lift coefficient compared to the baseline geometry. A 50% drag reduction was able to achieve with a partial section optimization compared to the baseline geometry.

Ikeda[15] evaluated the aerodynamic efficiency of a BWB aircraft with respect to an existing conventional aircraft, Airbus A380. Both the aircrafts were modelled using CAD tools analysed using CFD software. From the CFD results, BWB had 1.5 times higher L/D ratio than A380. Moreover, small drag value, less noise emission etc. make it more environmental efficient vehicle. Overall, a better aerodynamic and structural characteristic were reported than that of conventional aircraft for the same mission profile.

Richard J. Re[16] performed an experimental investigation to obtain force balance and wing pressure data on a 0.017 scaled model of an early blended-wing-body double deck subsonic transport configuration (without propulsion systems installation) with and without winglet. Tests were conducted in the Langley Research Center National Transonic Facility at low and high Reynolds numbers with Mach numbers within the range from 0.25 to 0.86. Results showed that at Mach number 0.25 and Reynolds number $2.5 \times 10^6$, the model remained stable up to a cl=1.4, after which the model became unstable and at Reynolds number $3.5 \times 10^6$, transition to instability was gradual and occurred at a lift coefficient of 1.1. At the cruise lift coefficient, the model was stable for all Mach numbers and Reynolds numbers.

Daniel J. Thompson[17] and his team constructed a 5m wingspan BWB UAV equipped with full navigation and autopilot system. The UAV was designed using 3D modelling and CFD analysis were performed to determine the aerodynamic characteristics at various angle of attack. Composite material was used as the material for the UAV since it has better strength to weight ratio than most metals. There main aim was to design a fully functional, efficient, applicable and practical for everyday use.

Sammi Ammar et al.[18] designed a 200 passengers capacity BWB aircraft and compared its aerodynamic performance with A320 aircraft with an emphasis on the stability of the aircraft. BWB aircraft's conceptual design was developed using the CEASIOM software. Aerodynamic results were obtained using TORNADO. Compared to A320, the BWB aircraft had an improved Lift-to-Drag ratio, indicating better performance than the former. The reason for the higher L/D ratio was because of the integration of wing with fuselage, creating large lifting surface. Hence, they concluded that the aerodynamic benefits seen in large BWB aircrafts are also applicable for small scale aircraft. The stability analysis showed that stability was also challenging in small scale model also. They were able to attain longitudinal stability but a lateral instability of the aircraft.

Biag AZ et al.[19] studied the aerodynamic characteristics and the stability analysis for a small scale BWB model. Analysis were done in XFLR5 which were then compared with FLUENT analysis and wind tunnel experiments. At small AoA till 10°, the CFD results were close match to the wind tunnel results but diverge at higher AoA. They reported that their designed model can be used for larger BWB which can be used as UAVs, carrying payload etc.

G. Larkin et al.[20] performed stability analysis of a Blended wing body with vertical stabilisers. Two baseline model were designed, one with vertically mounted twin-stabilisers, and another with inclined twin- stabilisers. Their results showed that vertical stabilisers are feasible in BWB configuration and will provide directional stability but also increases total drag.

M. Zhang et al.[21] presented an optimisation technique to minimise the cruise drag at transonic speed for a BWB configuration. They used a Euler solver and gradient-based optimisation. The optimised results showed a 45% reduction in the inviscid drag at designed lift.

Therefore, an enhanced performance of the BWB concept were confirmed from the review of the literatures. Computational analysis of BWB configuration will help in understanding the flow physics and the aerodynamic behaviour. An experimental validation with a 3-D model in a wind tunnel will be very useful and will provide a more accurate comparison of the obtained values

# CHAPTER 3

# RESEARCH METHODOLOGY

## OUTLINE

This chapter describes the methodologies used in the current project. The chapter is divided into two sections: experimental work and computational work. In experimental work, detail description of the experimental facilities, setups, instrumentations, details of the model used to carry out the experiment are given. In computational work, the computational approaches used for the BWB analysis are described in detail.

## 3.1 EXPERIMENTAL WORK

Experiments were carried out on a 3-D Blended Wing Body model. Quantitative and Qualitative analysis were performed at different angles of attack to study the flow physics of the BWB model. Quantitative analysis includes the measurement of forces and moments using 5-component strain gauge balance. Qualitative analysis was made using the tuft flow visualisation. The experiments were carried out from $\alpha=0^{o}$ to $\alpha=50^{o}$ with an increment of $5^{o}$ step.

### 3.1.2 Wind Tunnel Description

All experiments were conducted using low subsonic wind tunnel at the Aerodynamic Lab., Department of Space Engineering and Rocketry, BIT Mesra. This wind tunnel has a test section of 600mm x 600mm x 1200mm. It is a suction type, open circuit continuous flow fan driven wind tunnel. The flow velocity of the test section varies between 10-35m/s. The current experiments were performed at a velocity of 20m/s and Reynolds number of $2.1 \times 10^{5}$ based on the root chord. Figure 3.1 shows the low speed subsonic wind tunnel.


**Figure 3. 1:** Low subsonic wind tunnel

### 3.1.3 Model Description

The current BWB model was designed inspired from some of the measurements from the Roberto Merino Martinez's paper[8] and the aerofoil selections were based on the Martin Carlsson's ELSA BWB geometry[23]. Many design decisions were taken in order to improve the general performance of the BWB model. The geometry is composed of centre body, inner wing and an outer wing which were then "blended" to form the BWB. The propulsion systems are not included in the current BWB design, although its importance is fully appreciated.

The BWB model consists of 2 aerofoil profiles, NACA 0017 and NACA 0012, which are placed at 6 different sections, defining the geometry.

- NACA 0017, centre of the model, from 0mm to 0.35mm.
- NACA 0017, from 0.35mm to 41.5mm, comprising the fuselage
- NACA 0012, from 41.5mm to 52.28mm
- NACA 0012, from 52.28mm to 62.35mm, pair of inner wings
- NACA 0012, from 62.35mm to 82.21mm, comprising the outer wing
- NACA 0012, at the tip of the wing

Table 3.1 shows the specifications of the current BWB model. All the aerodynamic coefficients presented in this report are based on this reference area mentioned in Table 3.1.

**Table 3. 1:** Specifications of the current BWB model

| | |
|---|---|
| Root Chord Length | 157.14mm |
| Total Span (b) | 215.85mm |
| Aspect Ratio | 3.2 |
| Reference Area ($S_{ref}$) | 14547mm$^2$ |
| Sweep Angle (leading edge) | 71.66$^o$ |
| Sweep Angle (outer wing) | 38.52$^o$ |

### 3.1.3.1 Fabrication using 3D Printer

BWB model was designed as CAD model in SoildWorks and then imported to software for 3-D printing. Fused filament fabrication (FFF) process is used for the fabrication of the model. In fused filament fabrication, a filament of plastic material is fed through a moving heated head and is deposited on the platform, layer after layer, according to the shape given. The platform lowers after each layer is deposited. Acrylonitrile Butadiene Styrene (ABS) plastic is used for the fabrication of BWB model.

The BWB model was printed in two halves and then combined together to form the whole geometry. The model was coated with some layers of spray paint to increase the smoothness of the surface. Figure 3.2 shows the 3-D printer used for the fabrication of the model and the fabricated BWB model used of the experiment is shown in Figure 3.3.

To connect the model with the strain gage balance in the wind tunnel, a small mounting part was fabricated. One mouth of the mounting part was attached at the end of the BWB model and the other end was attached to the strain gauge balance. The model is then placed in the wind tunnel along with the strain gauge balance.


**Figure 3. 2:** 3-D Printer with the fabricated model

**Figure 3. 3:** BWB model placed in the wind tunnel.

### 3.1.4 Data Acquisition System

Data Acquisition is a process involving the sampling of signals that measure the physical values from different measuring instruments and converting the resulting samples into digital numeric values that can be manipulated by a processing system. The DAQ systems convert analog waveforms into digital values for processing.

NI DAQ (PCI - 6036E) card was used having a 16-bit resolution. It consists of 16 single ended and 8 differential inputs with a maximum sampling rate of 200 KS/s. The input range is $\pm 0.05$ to $\pm 10V$. The card is provided with an absolute accuracy of 0.0611mV in the input range of $\pm 50.0$mV.

### 3.1.5 Model Mounting and Incidence Mechanism

The model mounting mechanism used was a HOLMARC Pitch and Yaw Positioning Mechanism Model no. HO-PY-WT01 shown in Figure 3.4 which provided the facility of both mounting the model and controlling the angular motion of the model in the pitching and yawing plane. The motion of the incidence mechanism was controlled electronically controlled using the Micro Position Controller model no. HO-SPC-3H. The pitch angle can be varied in between the range of 0° to 75° and the yaw angle in the range of $\pm 20°$. The data inputs to the incidence mechanism are transferred through the micro position controller in the form of numerical values given to its software installed in a computer. A base plate was inserted into the downward side of the test section with a rectangular cavity to insert the mounting end of the incidence mechanism inside the test section. The total blockage ratio due to the mounting end of the incidence mechanism was less than 2% in the test section.

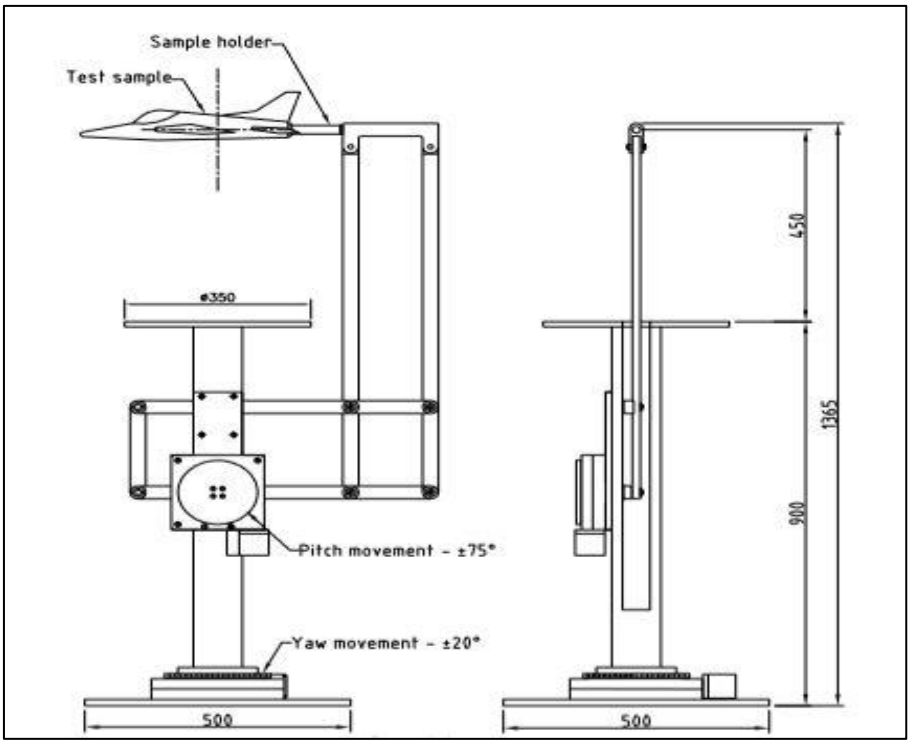


**Figure 3. 4:** Schematic of the mounting mechanism[27]

### 3.1.6 Force Measurement

The model forces and moments were measured using a 5-component strain gage balance mounted in the wind tunnel. A 5-component strain gauge will measure three forces (axial, normal and side force) and two moments (pitching moment and yawing moment) acting on the model.

#### 3.1.6.1 Strain Gauge

A Strain gauge is a device used to measure the strain acting on the body. It works on the principle of Wheatstone bridge. It consists of 4 resistors, out of which two are known, one is a variable resistor and one is unknown. Figure 3.5 shows the 5-component strain gauge balance

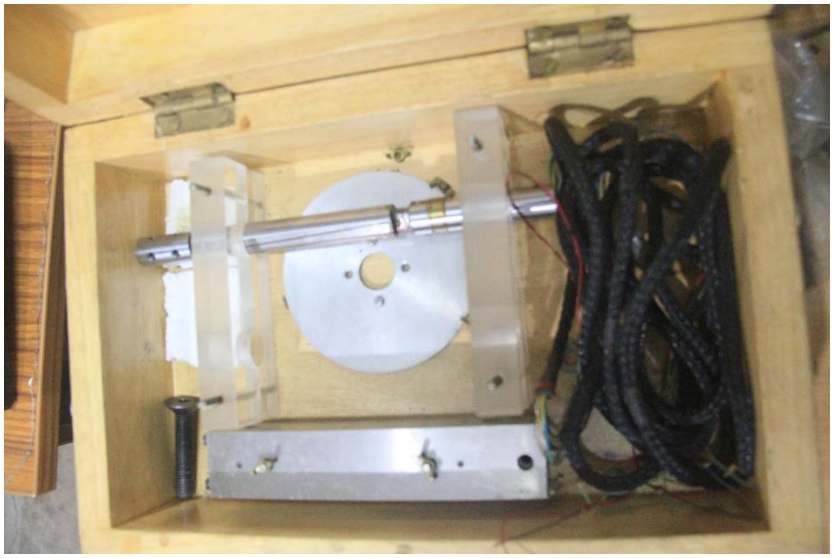

**Figure 3. 5:** 5-component strain gauge balance

#### 3.1.6.2 Principle of Strain Measurement

Strain initiated resistance change is extremely small. Therefore, for the strain measurement, a wheat stone bridge is formed to convert the resistance voltage change. If R1, R2, R3, R4 are the resistances and E is the bridge voltage, then the output voltage is obtained by the following equation:

$$V_o = \frac{R1*R3-R2*R4}{(R1+R2)(R3+R4)} * E \qquad \text{....3.1}$$

Suppose there is change in resistance due to the strain, then the output voltage becomes,

$$V_o = \frac{(R1+\Delta R)*R3-R2*R4}{(R1+\Delta R+R2)(R3+R4)} * E \qquad \text{....3.2}$$

Thus, the result obtained is the voltage that is proportional to change in resistance i.e. change in strain.

#### 3.1.6.3 Estimating Forces

The data obtained from the strain gauge balance was in the form of matrix. The forces were then calculated by multiplying the matrix with the inverse of coefficient of the matrix provided by the manufacturer.

$$[F] = [A^{-1}][O] \quad \text{....3.3}$$

where $[O]$ is the matrix obtained from the strain gauge in millivolts (mV),$[A]$ is the coefficient matrix provided by the manufacturer, and the $[F]$ is the force matrix.

The normal force and axial force were calculated using:

Normal force (N) = $N_1$+$N_2$

Axial force (A) = $A_1$+$A_2$

And the forces coefficients

Normal Coefficient $C_N = \frac{N}{q_\infty S_{ref}}$

Axial Coefficient $C_A = \frac{A}{q_\infty S_{ref}}$

where $q_\infty$ the dynamic pressure and $S_{ref}$ is the reference area of the model.

The lift and drag coefficients were then obtained using the following formula:

$C_L = C_N\cos\alpha - C_A\sin\alpha$ ....3.4

$C_D = C_N\sin\alpha + C_A\cos\alpha$ ....3.5

### 3.1.7 Flow Visualisation

Flow visualisation techniques are used to visualise how the flow moves over and around the model. Some of the flow visualisation techniques commonly used in subsonic wind tunnel are:

- Oil Flow Visualisation
- Smoke Flow Visualisation
- Tuft Flow Visualisation

For the current experiment, tuft flow visualisation was used. Tufts are small, light and flexible strings usually made of nylon or cotton. These tufts were stuck on to the model surface using glue. The orientation of tufts with respect to the freestream flow indicates the flow features like flow separation, reattachment and recirculation region.

### 3.1.8 Experimental Plan of Work

The experiments for the quantitative and qualitative analysis were carried out on the fabricated BWB model in the low subsonic wind tunnel at different angles of attack. Table 3.2 show the details of the test plan.

**Table 3. 2:** Test Plan for the Experiments

| Model | Experiments | Angles of attack |
|---|---|---|
| BWB model | Force measurements | $\alpha = 0^o,5^o,10^o,15^o,20^o,25^o,30^o,35^o,40^o,45^o,50^o$ |
| | Tuft flow visualisation | $\alpha = 0^o,5^o,10^o,15^o,20^o,25^o,30^o,35^o,40^o,45^o,50^o$ |

## 3.2 COMPUTATIONAL WORK

To study the flow over the model, computational analysis over the model were performed. OpenFOAM, a free, open source software package was used to simulate the flow over the blended wing body at different angles of attack.

The computational process for the BWB analysis is divided into three phases:

**Phase 1:** Model designing using CAD software, SolidWorks 2018.

**Phase 2:** Mesh generations using GAMBIT.

**Phase 3:** Numerical simulation using OpenFOAM.

Since running a simulation in OpenFOAM is very different from that of the commercial software, hence to familiarise and validate the OpenFOAM setups, some standard 2-D cases were simulated first. The test cases were chosen in such a way that the validation of the results was possible. Some test cases were chosen to check whether a particular approach was possible for the 3-D case as well. The standard cases for the simulation are given below:

- Incompressible, laminar case, 2-D cylinder case
  - $M_\infty$ = 0.1, Re = 40, α = 0°
  - simpleFoam solver
- Compressible, subsonic, turbulent case, RAE 2822 2-D Aerofoil
  - $M_\infty$ = 0.675, Re = 6.5 million, α = 1.92°
  - $y^+ = 1$, $y^+ = 50$.
  - rhoCentralFoam solver
  - Spalart-Allmaras Turbulence model.

This helped in understanding the file structures and working of OpenFOAM and some of the conclusions made from these cases were used during the 3-D BWB case.

### 3.2.1 CAD Modelling

Firstly, a 2-D outline of a half-blended wing body configuration was designed in the SoildWorks. The aerofoils coordinates were then generated[28] and imported at 6

different sections of the geometry and were blended to form one surface. The half model was used for the computations whereas a full model was generated using the mirror function. The full model was used in the experiments. Detailed sketch of the final BWB is shown in Figure 3.6. Different views of the final geometry are shown is the Figure 3.7.

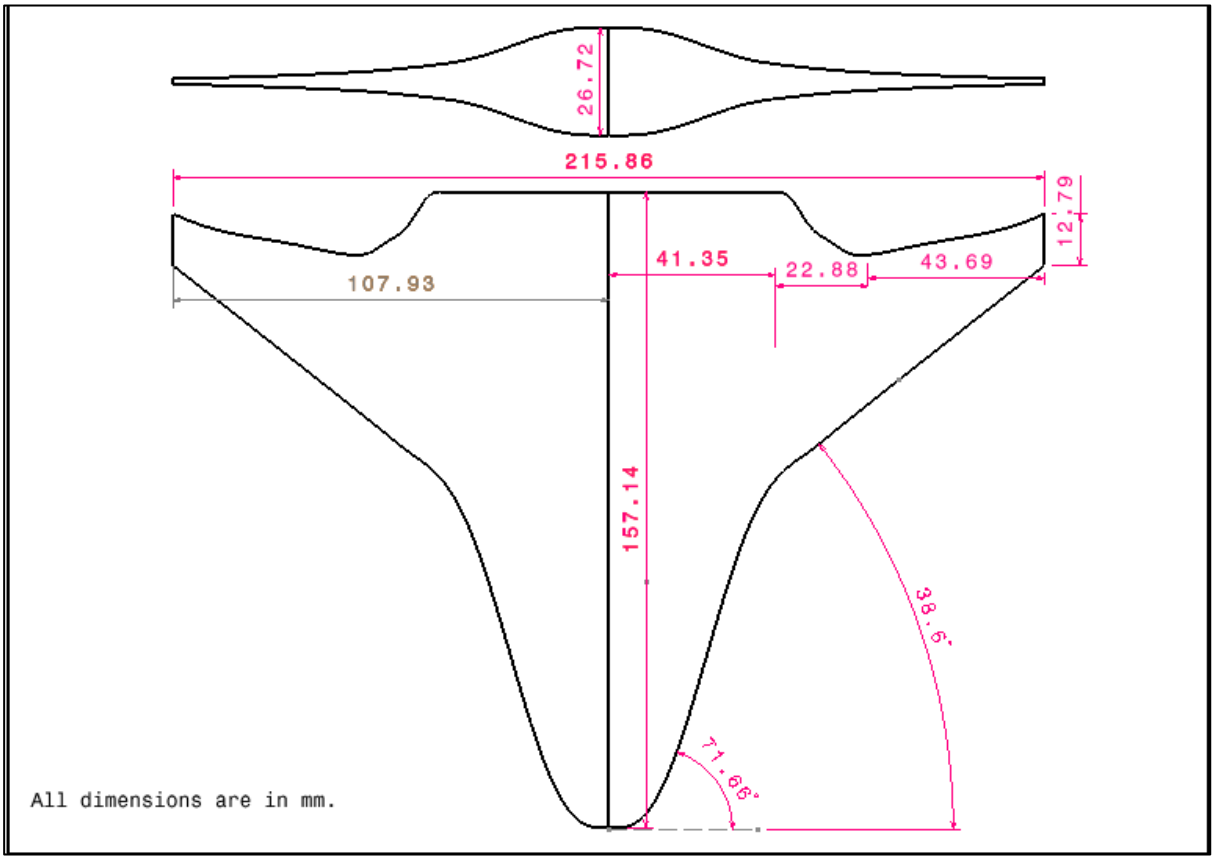


**Figure 3. 6:** Detailed sketch of the BWB model

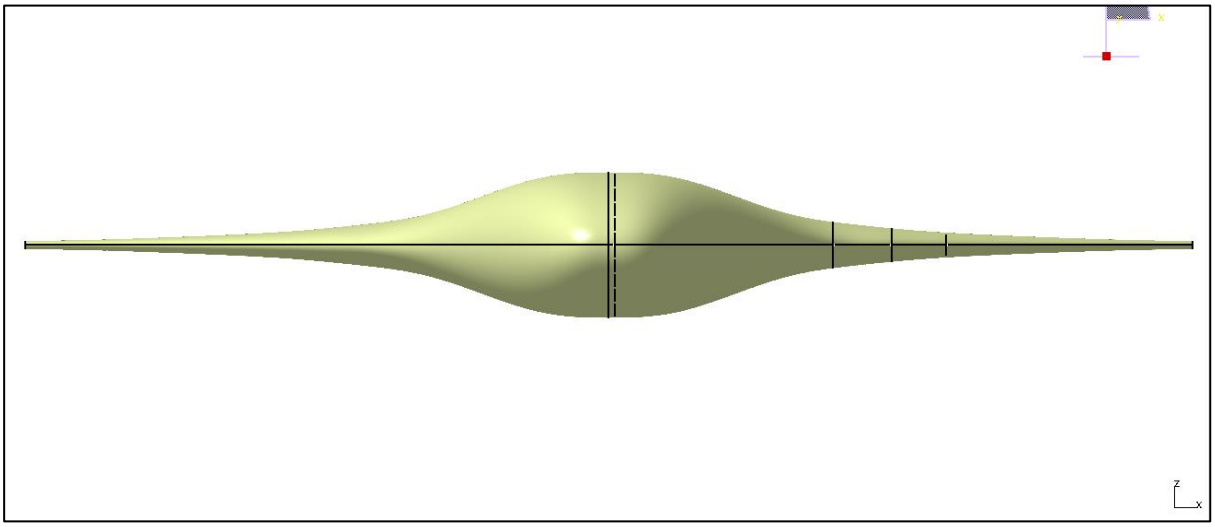

(a) Front View

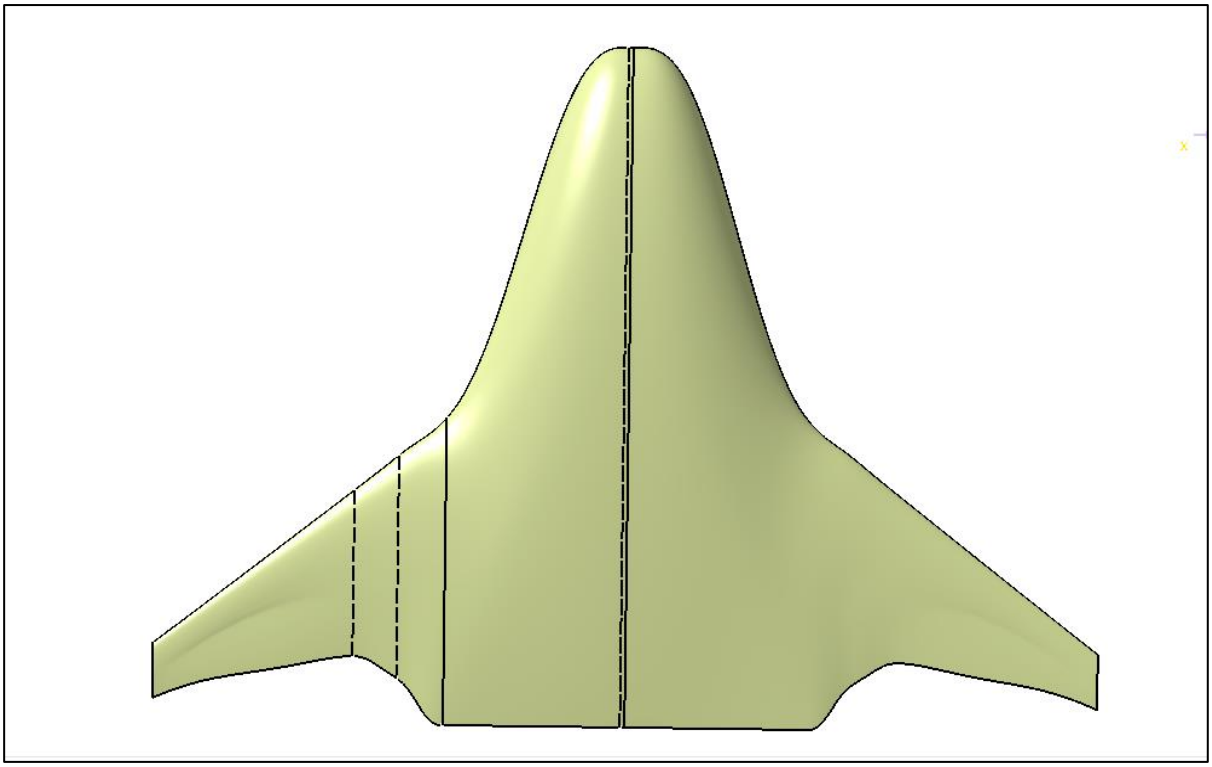

(b) Top View

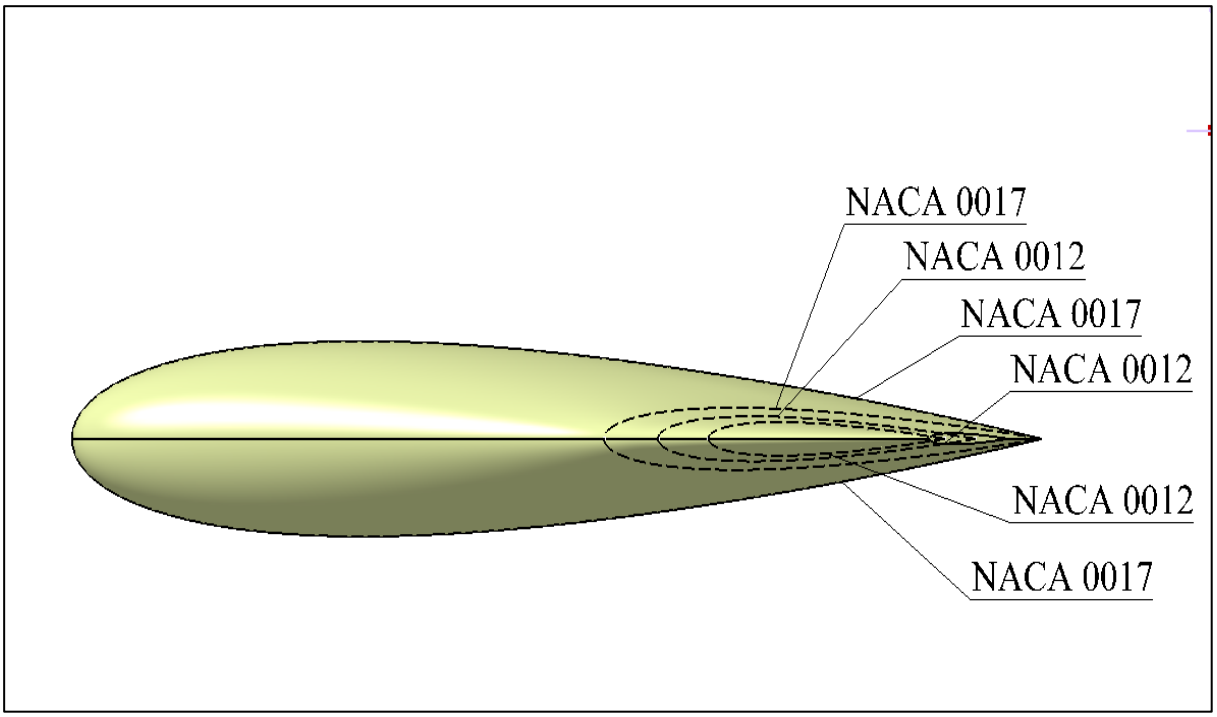


(c) Side View

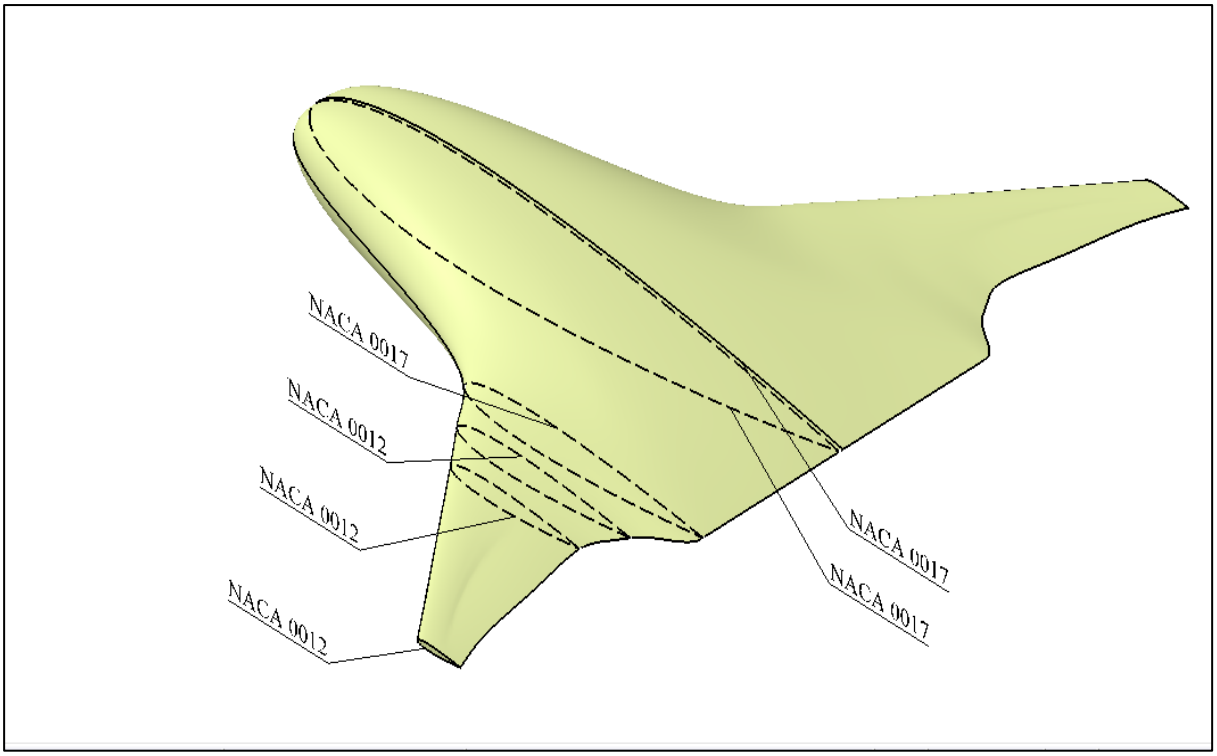


(d) Isometric View

**Figure 3. 7:** Different views of the BWB model

### 3.2.2 Mesh Generation

The half model designed in the SolidWorks was then imported into the meshing software, GAMBIT. Two C-type grid domains were generated around model to produce a structured grid in domain as shown in Figure 3.8. The outer domain was 20 times the total chord of the blended wing body. Grid stretching was used to concentrate the mesh accordingly over the model and domain. The grid used for the simulation is hexahedral structured grid everywhere except the tip of the wing where hex/wedge type with cooper scheme grid was generated. The adjacent plane to the model act as symmetry plane. Figure 3.9 shows a closer view of the mesh on the model. The mesh contains 2.1 million cells and was designed considering the use of a wall function. The y+ value of the first grid point off the wall was taken as 50. The boundary conditions specified for the grid are shown in Figure 3.10. The meshes were then converted to OpenFOAM format by giving the *fluent3DMeshToFoam* command in the terminal.

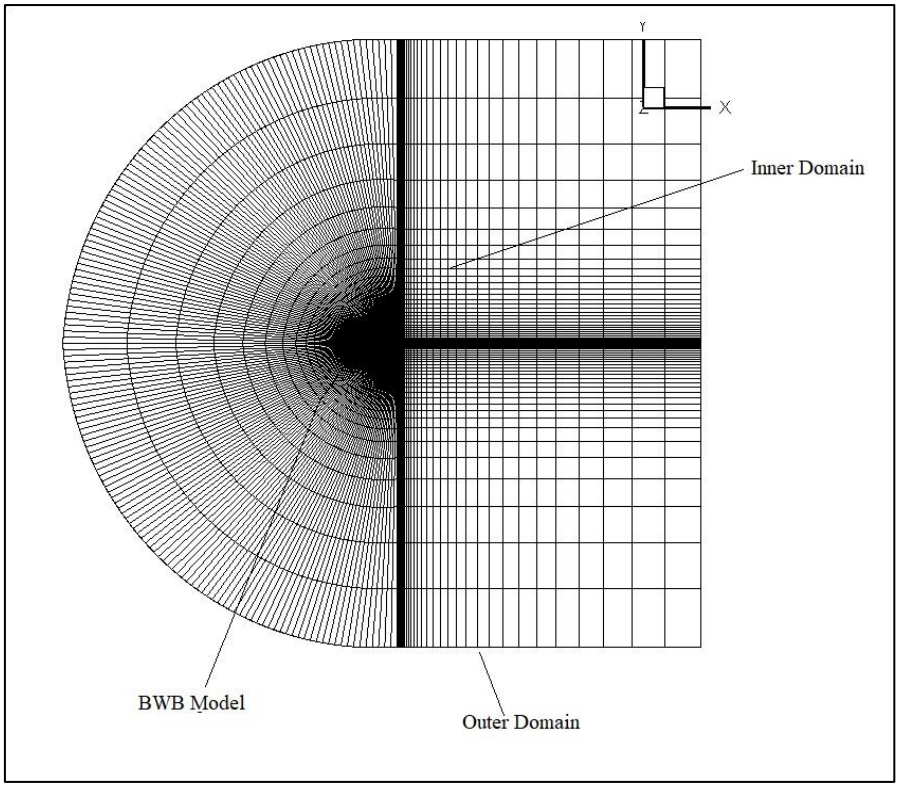


**Figure 3. 8:** Computational Domain

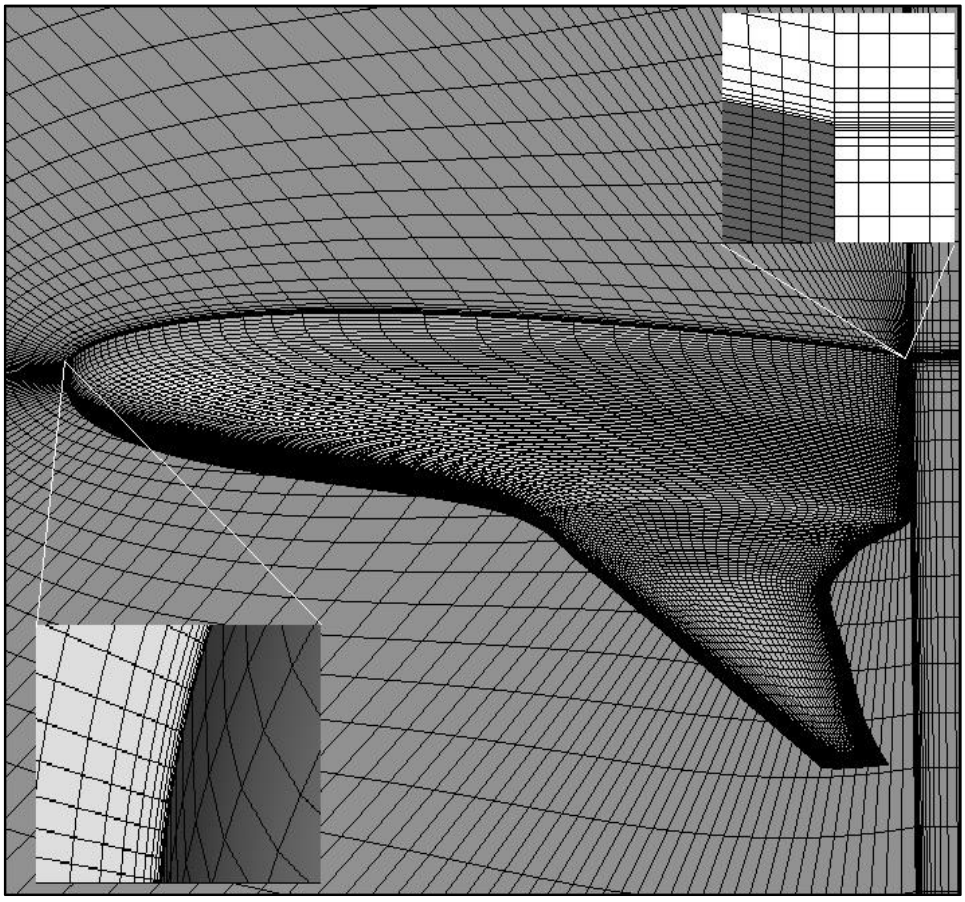

**Figure 3. 9:** Closer view of the mesh over the model

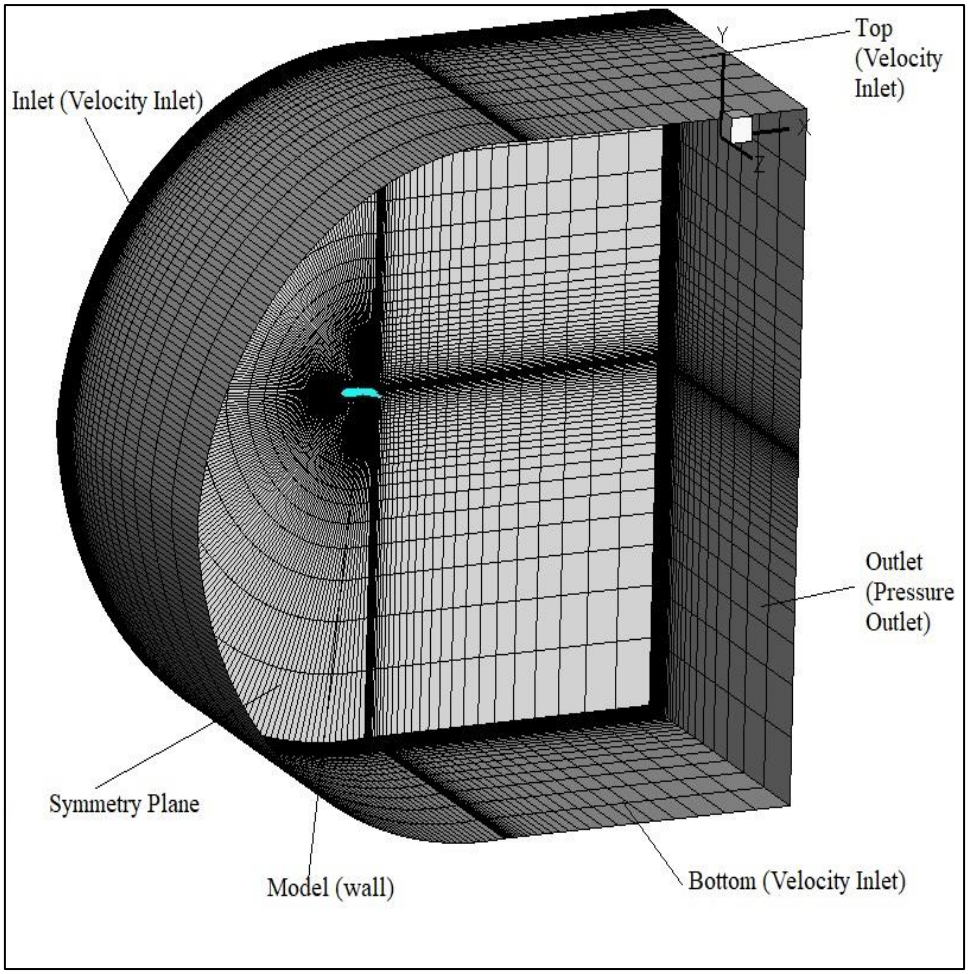


**Figure 3. 10:** Boundary conditions used for the domain

### 3.2.3 Boundary Conditions

The standard Dirichlet and Neumann boundary conditions were used for all the simulations. A velocity inlet boundary condition was given at the inlet, top, and bottom and side of the domain. At the outlet, a pressure outlet boundary condition was given. At the surface of the model, the velocity was set to be zero, giving a no slip condition and for the adjacent side of the model, it was set to SymmetryPlane. Simulations were performed at a flow speed of 20 m/s. Initial values for nut and nuTilda were calculated using eq. 3.11 and eq. 3.12 respectively. In OpenFOAM, all the boundary conditions and initial conditions are entered in text format into the files present in the 0 directory. The details of these files are shown in Appendix.

### 3.2.4 Mathematical Modelling in OpenFOAM

#### 3.2.4.1 Governing Equations

For an incompressible flow, the continuity and Navier-Stokes equations are:

$$\nabla . U = 0 \quad \text{....3.6}$$

$$\frac{\partial U}{\partial t} + \nabla . (UU) = -\frac{1}{\rho}\nabla p + \nabla . (\nu \nabla U) + \frac{F}{\rho} \quad \text{....3.7}$$

These equations are very difficult to solve numerically because:

- There are equations for velocities but no direct equation for calculating the pressure.
- Non-linearity in the equation.
- The velocity field calculated from the momentum equations must satisfy the continuity equation.

Hence, SIMPLE algorithm was used which derives an equation for pressure and a corrector for the velocity field.

### 3.2.5 Turbulence Modelling

At low Reynolds number, the flow is laminar and as the Reynolds number increases, the flow changes from laminar to turbulent. In real life, most of the flow are turbulent in nature. Hence turbulence models are used to resolve turbulence in the flow during simulations to give accurate results matching the actual real-life flows. To simulate turbulent flows, several approaches are available in OpenFOAM like (Reynolds averaged Navier-Stokes) RANS, Detached Eddy Simulation (DES), Large Eddy Simulation (LES), Direct Numerical Simulations (DNS) etc. and are considered based on the level of accuracy needed and the computational capabilities. For the current simulation, RANS with SA model was used.

#### 3.2.5.1 Spalart-Allmaras (SA) Turbulence Model

Spalart-Allmaras (SA) model is a one equation model which solves a modelled transport equation for nut (kinematic turbulent eddy viscosity)[22].SA model was designed specifically for aerospace applications has shown good results for aerodynamic flows.

The final form of the one-equation model is expressed as

$$\frac{\partial \widetilde{\nu_T}}{\partial t} + \frac{\partial}{\partial x_j}\left(\widetilde{u_j}\widetilde{\nu_T}\right) = c_{b1}[1 - f_{t2}]\tilde{S}\widetilde{\nu_T} - \left[c_{w1}f_w - \frac{c_{b1}}{k^2}f_{t2}\right]\left[\frac{\tilde{\nu}_T}{d}\right] + \frac{1}{\sigma}\left[\frac{\partial}{\partial x_j}\left((\nu + \tilde{\nu}_T)\frac{\partial \tilde{\nu}_T}{\partial x_j}\right) + c_{b2}\left(\frac{\partial \tilde{\nu}_T}{\partial x_j}\frac{\partial \tilde{\nu}_T}{\partial x_j}\right)\right] + f_{t1}\Delta U^2 \quad \ldots.3.8$$

where

$$f_{t1} = c_{t1}g_t \exp\left(-c_{t2}\frac{\Omega_t^2}{U^2}[d^2 + g_t^2 d_t^2]\right) \quad \ldots.3.9$$

$$f_{t2} = c_{t3}\exp(-c_{t4}\mathcal{X}^2) \quad \ldots.3.10$$

and the constants are:

$c_{b1} = 0.1355$

$c_{b2} = 0.622$

$\sigma = 2/3$

$k = 0.41$

A modified eddy viscosity, nuTilda is initialised by

$$\widetilde{\nu_T} = \frac{3\mu}{\rho} \quad \ldots.3.11$$

The relationship between the variables $\widetilde{\nu_T}$ and $\tilde{\nu}$ is given by

$$\widetilde{\nu_T} = \tilde{\nu}f_{v1} \quad \ldots.3.12$$

where,

$$f_{v1} = \frac{\chi^3}{\chi^3 + c_{v1}^3}$$

$$\chi = \frac{\widetilde{\nu_T}}{\nu}$$

and $\rho$ is the density, $\nu = \frac{\mu}{\rho}$ is the kinematic viscosity, and μ is the dynamic viscosity. $c_{v1}$ is a constant.

In OpenFOAM, the physical properties of the fluid were set in the transportProperties for an incompressible flow, and the turbulence model was set in the turbulenceProperties file present in the constant directory. The files in the constant directory is shown in Appendix.

### 3.2.6 Wall Functions

In turbulent flow simulations, two approaches can be taken in the near-wall regions. First one is to generate a fine mesh near the wall region such that the first cell is placed in the viscous sublayer region. This method will increase the computational time significantly since the mesh is very fine. Another way is to use the wall functions. Wall functions are empirical equations which satisfy the physics of the flow near the wall region. With the use of wall functions, there is no need to use fine mesh since the boundary layer are no longer needed to be resolved.

To define a wall function properly, $y^+$ is need to be determined. $y^+$ is a non-dimensional number which will give the distance of the first cell from the wall.

$$y^+ = \frac{y * u_\tau}{\nu} \quad \text{....3.13}$$

$$u_\tau = \sqrt{\frac{\tau_w}{\rho}} \quad \text{....3.14}$$

where $u_\tau$ is the friction velocity, y is the distance to wall and $\nu$ is viscosity of the fluid.

If the value of $y^+$ is less than 5, the first cell lies in the viscous sublayer and the mesh is fine enough and wall functions are not necessarily needed. A wall function simulation normally requires that $y^+$ of the first cell outside the walls is in the log-layer, which starts at about $y^+$= 30 and, depending on the Re number, extends up to say $y^+$= 200. The first cell is usually avoided in between the $y^+$= 5 to 30, called the buffer region, since it exhibits complex velocity profile.

For the current project, all simulations were done with of $y^+$ value of 50 and wall function nutUSpaldingWallFunction was implemented.

### 3.2.7 Solver Settings

In OpenFOAM, the solver specifications were given through the fvScheme file present in the system folder. The solver used for the BWB simulation was *SimpleFoam.* The different numerical schemes used are given in Table 3.3.

**Table 3. 3:** Numerical Schemes used for the simulation

| **Gradient Scheme** | |
|---|---|
| Default | cellLimited leastSquares 1.0 |
| **Laplacian Schemes** | |
| Default | Gauss linear limited 0.33 |
| **Divergence Schemes** | |
| $\phi$U | Gauss linearUpwind grad(U) |
| $\tau_{MC}$ | Gauss linear |
| **Time Scheme** | |
| Default | steadyState |
| **Surface Normal Gradients** | |
| Default | limited 0.33 |
| **Interpolation Schemes** | |
| Default | Linear |

The equation solvers, tolerances and algorithms were defined in the fvSolution file. For solving the pressure equation, generalized Geometric-Algebraic Multi-Grid (GAMG) solver (GAMG) with a tolerance of $1e^{-5}$ and *GaussSeidel* as smoother was used. GAMG is faster than standard methods when the increase in speed by solving first on coarser meshes. For U and nuTilda equation, *smoothSolver* was used with a tolerance of $1e^{-8}$ and *GaussSeidel* as smoother. Under-relaxation factors were controlled using *relaxationFactors*. The factors specified for pressure, velocity, and turbulent fields were 0.3, 0.7, 0.7 respectively. The files present in the system directory are given in Appendix.

### 3.2.8 Running Simulation

Simulation in OpenFOAM are run by inputting specific commands in the Linux terminal. Once all the data were entered in each file, before running the simulation, enter the following commands are given in the terminal:

> *checkMesh*: To examine the quality of the mesh.

- *transformPoints –scale '(0.001 0.001 0.001)':* To scale down the domain of the mesh by $10^3$ (mesh is scaled down in meters from millimetres).
- *renumberMesh –overwrite:* Reduces the bandwidth of the coefficient matrices by renumbering the cell list.

Parallel processing in OpenFOAM is done using MPI. To run the case in parallel processing, decomposeParDict file is needed in the folder system. In this file, the number of subdomains and the method of decomposition is defined. To run the simulation in parallel mode using simpleFoam solver, enter the following command in the terminal:

- *decomposePar:* To divide the domain into different subdomains for parallel simulation.
- *mpirun –np 4 simpleFoam –parallel:* runs the simulation in parallel.
- *reconstructPar:* To combine results of all the subdomains after the simulation.

### 3.2.9 Post Processing

#### 3.2.9.1 Calculation of Force coefficients

To calculate the force coefficients on the model, function objects are called as the simulation runs. These function objects are small, independent codes compiled into OpenFOAM libraries and are written in the controlDict file. These codes run at the end of each iterations and monitor the simulation as it runs. The script used to calculate the force coefficient at $\alpha = 0^{o}$ is given below. The following code will calculate the lift, drag and moment coefficients at end of each iterations as the simulation proceeds. Similarly, for each angle of attack, the force coefficients were obtained by changing the liftDir and dragDir accordingly.

```
functions
{
forceCoeffs
  {
    type forceCoeffs;
    libs ("libforces.so");
    patches (bwb);
    rhoInf 1.225;
    rho rhoInf;
    log true;
    CofR (0.25 0 0);
    liftDir (1 0 0);
    dragDir (0 1 0);
    pitchAxis (0 0 1);
    magUInf 20;
    lRef 0.15714;
    Aref 0.01454;
    writeControl timeStep;
    timeInterval 1;
  }
};
```

#### 3.2.9.2 ParaView

Most of the post processing work were done using the Paraview software. Paraview is open-source software used for data analysis and visualisations. The data obtain from the simulations were imported into ParaView. Different contours for pressure, velocity, path lines, streamlines, etc. were extracted from the data obtained. Values of pressure and velocity at each point on the model can be extracted in spreadsheet format. Pressure coefficient (Cp) were obtained at different span wise location of the model for different angles of attack. The value of Cp plots were also collected in spreadsheet format.

### 3.2.10 Computational Plan of Work

The computational analysis was carried out using OpenFOAM. The BWB half model was simulated at different angles of attack for the quantitative and qualitative analysis. The results were then compared with the experimental results. Table 3.4 show the angles of attack at which the computation was done.

**Table 3. 4:** Test plan for the Computation

| **Model** | **Computations** |
|---|---|
| BWB half model | $\alpha$ = 0º, 5º, 20º, 25º, 30º, 35º, 40º, 45º, 50º, 60º |

# CHAPTER 4

# RESULTS AND DISCUSSION

## OUTLINE

This chapter presents the results obtained from the CFD and the experimental analysis of the Blended wing body configuration. The quantitative and qualitative analysis are carried out to study the aerodynamic behaviour of the Blended wing body at subsonic speed. Quantitative analysis includes force measurements, pressure distribution over the surface of the model. Qualitative analysis includes tuft flow visualisation. The results obtained are analysed and discussed in detail to understand the flow behaviour over the BWB model. The CFD results are then compared with the experimental results.

Validation results of standard cases simulated using OpenFOAM are also present in this section.

## 4.1 STANDARD TEST CASES FOR VALIDATION

Standard test cases were simulated to check the reliability of the OpenFOAM software in predicting the aerodynamics coefficients and contours.

### 4.1.1 CASE 1: Incompressible and laminar flow over 2-D cylinder case

Incompressible and laminar flow over 2-D cylinder was simulated at a Mach number of 0.1 and Reynolds number 40 using simpleFoam. Figure 4.1 and Figure 4.2 show the Mach number and pressure contour of the cylinder from the CFD analysis. Figure 4.3 shows the comparison of the pressure coefficient obtained from the CFD analysis and the experimental data[24]. The Cp distribution compares closely with the experimental data and it validates the SimpleFoam for incompressible flow simulation. Hence simpleFoam solver is made use of for incompressible cases.

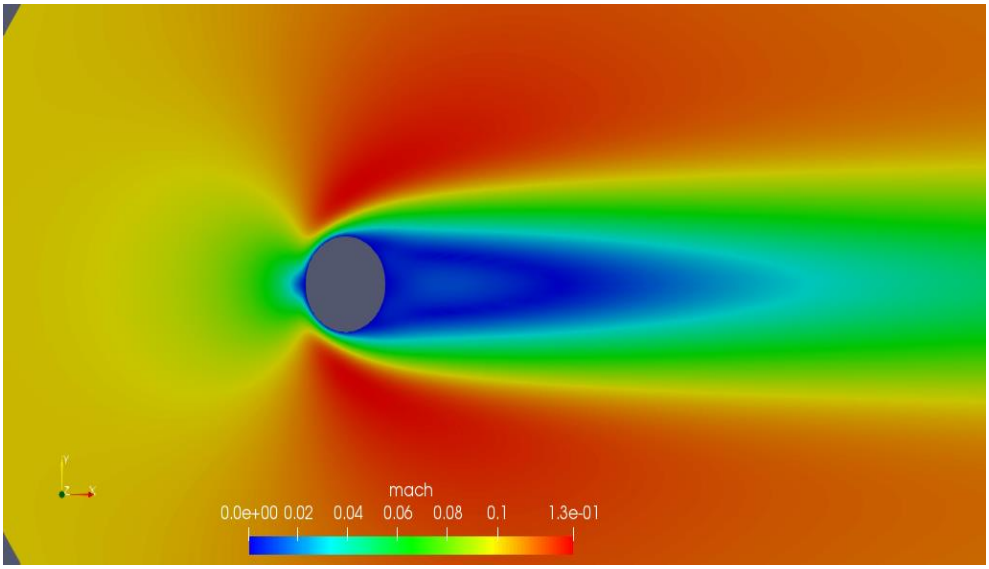


**Figure 4. 1:** Mach contour over the cylinder (M=0.1, Re=40)

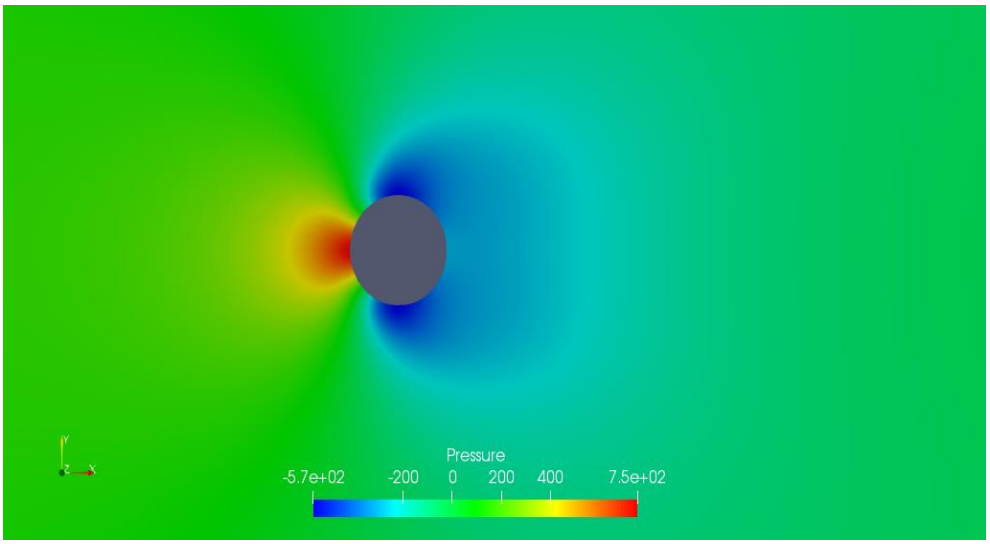


**Figure 4. 2:** Pressure contour over the cylinder (M=0.1, Re=40)

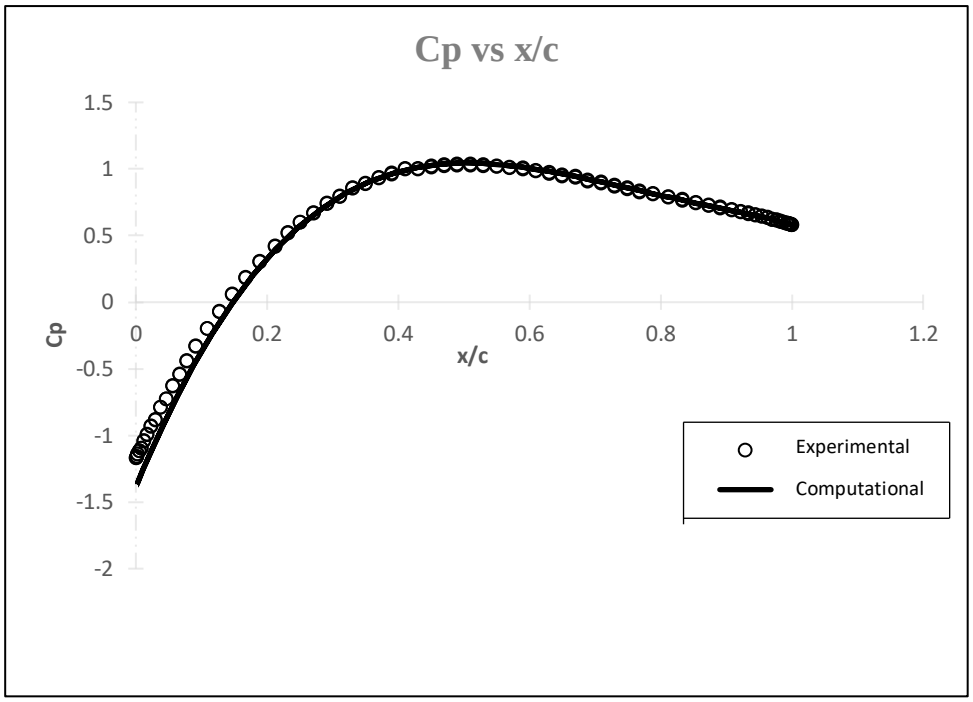


**Figure 4. 3:** Cp distribution over the cylinder (M=0.1, Re=40)

### 4.1.2 CASE 2: Compressible, subsonic and turbulent flow over RAE 2822 2-D aerofoil

A 2D aerofoil was simulated at a Mach number of 0.675 and Reynolds number of 6.5 million at an angle of attack of 2.79° using rhoCentralFoam. Two different meshes were generated, one with a $y^+$ value of 1 and another with a $y^+$ value of 50. A wall function was used for $y^+ = 50$ grid with the Spalart-Allmaras turbulence model for turbulent flow simulation. Figure 4.4 and Figure 4.5 shows the Mach number and pressure contour from the CFD analysis. Figure 4.6 shows the comparison of the pressure coefficients obtained for $y^{+1}$ and $y^{+50}$ grids and the experimental data[25].The Cp distributions for both the $y^+$ values were in close agreement with the experimental data.

This numerical experiment confirms that the wall function approach can be used to reduce the mesh size. Therefore, $y^+= 50$ grid with wall function is used for the BWB geometry. Moreover, the results for the present CFD simulations helped in choosing and finding a correct set-up for turbulence model and a good solver setting in OpenFOAM for the 3-D BWB case.

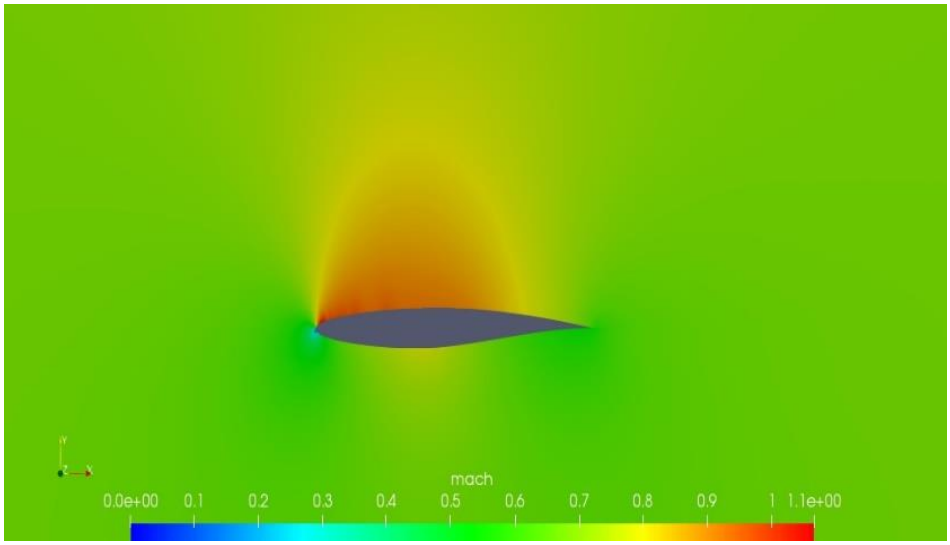


**Figure 4. 4:** Mach contour over RAE 2822 airfoil (M=0.675, Re=6.5 million)

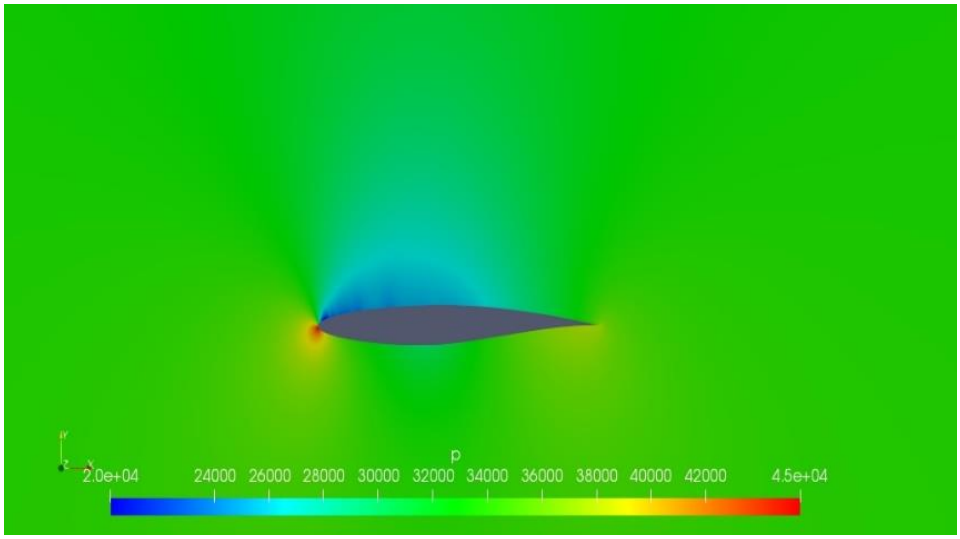


**Figure 4. 5:** Pressure contour over RAE 2822 aerofoil (M=0.675, Re=6.5 million)

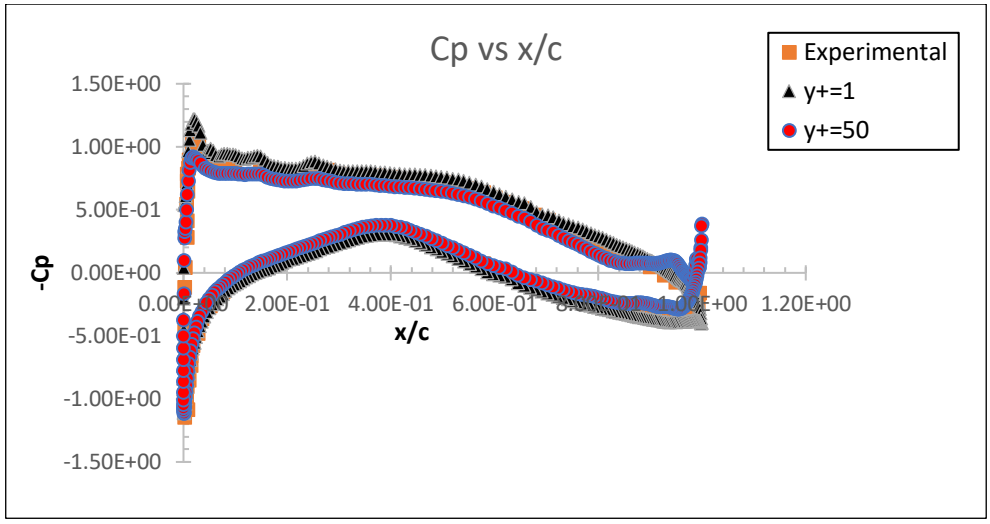


**Figure 4. 6:** Comparison of Cp distribution over RAE 2822 aerofoil for different y+ value (M=0.675, Re=6.5 million)

## 4.2 AERODYNAMIC CHARACTERSITICS OF BWB

The primary objective of the thesis was to study the aerodynamic characteristics of the BWB model at different angles of attack at low subsonic speed. Hence CFD analysis were carried out using OpenFOAM software.

### 4.2.1 Force Coefficients

Aerodynamic force coefficients which includes the lift coefficient and the drag coefficient acting over the model were computed for the different angle of attack.

Figure 4.7 shows the variation of the lift coefficient ($C_L$) for different angles of attack ($\alpha$) varying from 0º to 60º obtained from the CFD analysis. Since all the aerofoil profiles in the BWB model are symmetric at 0º, the $C_L$ is nearly zero. The curve then increases almost linearly with the increase in angle of attack up to 40º. At higher angles, the vortex core is energised, the velocity in the vortex increases, hence the pressure is low. This low pressure on the upper surface will produces lift. Increasing the angle of attack beyond 45º, the flow will fully separate from the. At this point, the $C_L$ starts decreasing with the angle of attack, and the body said to be stalled. The BWB model is stalled at AoA of 45º.

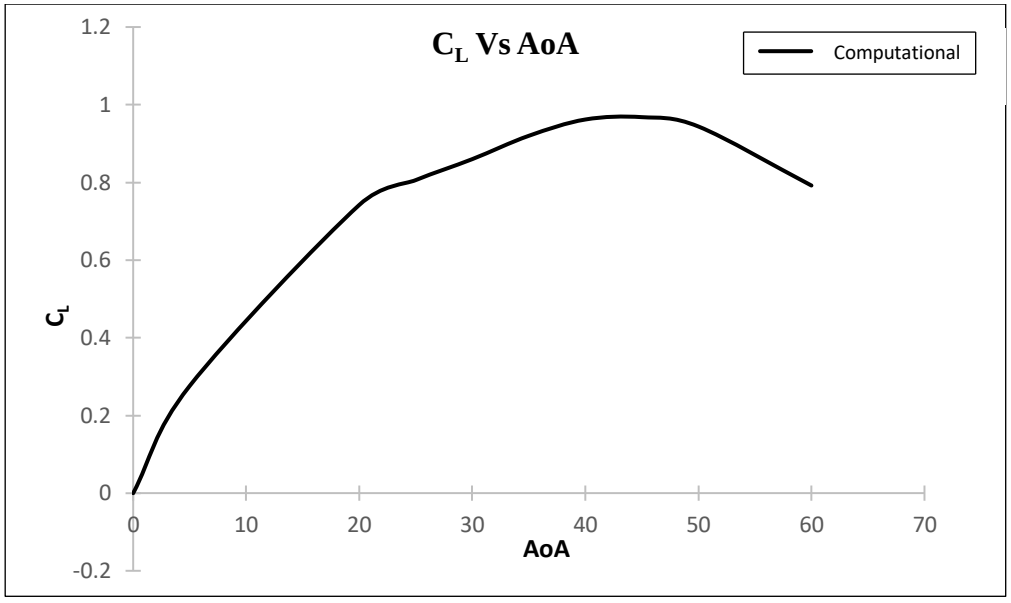


**Figure 4. 7:** Variation of Lift Coefficient with angle of attack for BWB ($U_\infty$=20m/s, Re=2.1x$10^5$)

Figure 4.8 shows the variation of the drag coefficient ($C_D$) for different angles of attack (α) varying from 0º to 60º obtained from the CFD analysis. At low angles of attack (α < 10º), the value of $C_D$ is small and the variation of $C_D$ is almost constant with the angle of attack. This is because, at low angle of attack, the flow is still attached to the wing and body. As the angle of attack increases from α = 10º, $C_D$ also increases and will continue to increases. At low angles of attack, skin friction drag will be dominant as compared to pressure drag on the body, therefore the increase in drag is also low but at high angles of attack, pressure drag starts increasing more due to flow separation which explains the increase in the drag.

The Lift to Drag ratio (L/D) is the amount of lift generated by a wing compared to its drag. A ratio of L/D indicates aircraft efficiency and performance. Aircraft with higher L/D ratios are more efficient. Figure 4.9 shows the variation of the Lift to Drag ratio (L/D) for different angles of attack (α) varying from 0º to 60º obtained from the CFD analysis. The maximum value of L/D is achieved at an angle of attack of 6º. Hence the optimum flight configuration of the BWB body is at α = 6º.

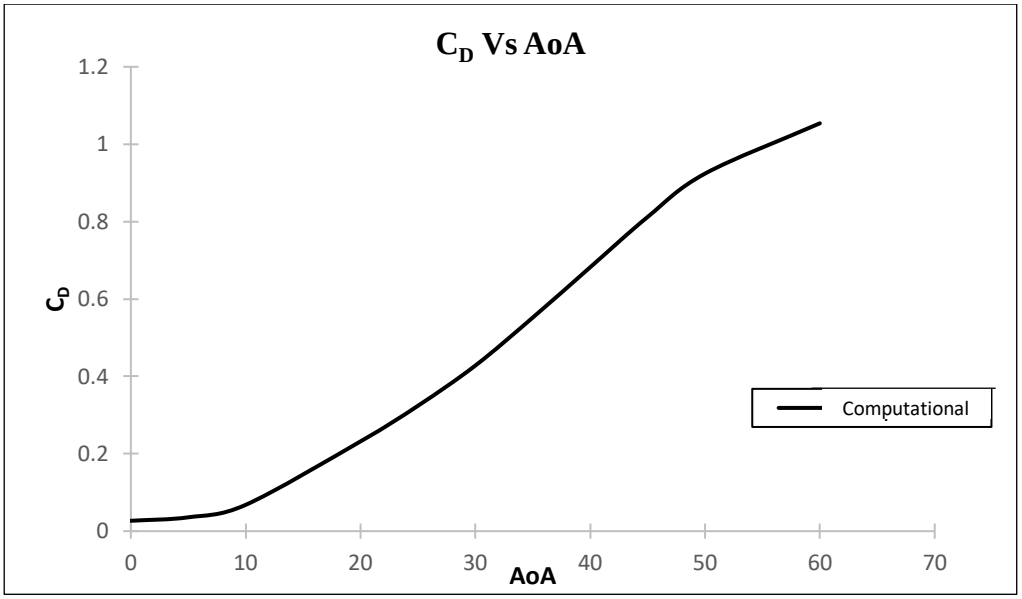


**Figure 4. 8:** Variation of Drag Coefficient with angle of attack for BWB ($U_\infty$=20m/s, Re=2.1x$10^5$)

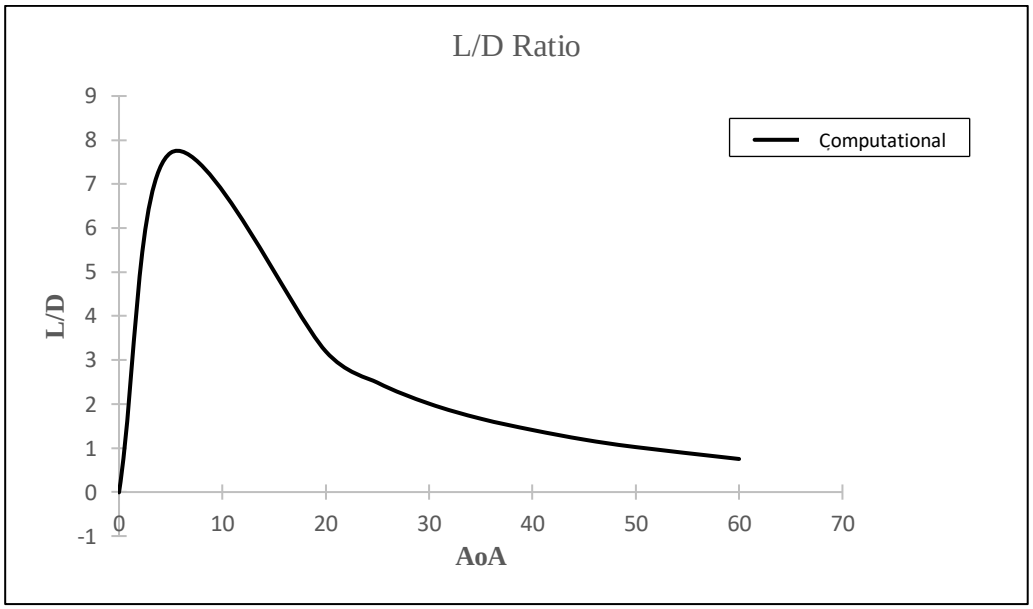


**Figure 4. 9:** Variation of L/D with angle of attack ($U_\infty$=20m/s, Re=2.1x$10^5$)

Drag polar gives the relationship between the drag coefficient and the lift coefficient. Figure 4.10 shows the drag polar for the BWB model. Initially, the lift coefficient changes exponentially with the drag coefficient, later on the lift coefficient almost becomes constant with the increasing drag coefficient. This trend is because at high angles of attack, separation occurs, due to which the pressure drag increases. Therefore, the total drag acting on the model is also increased.

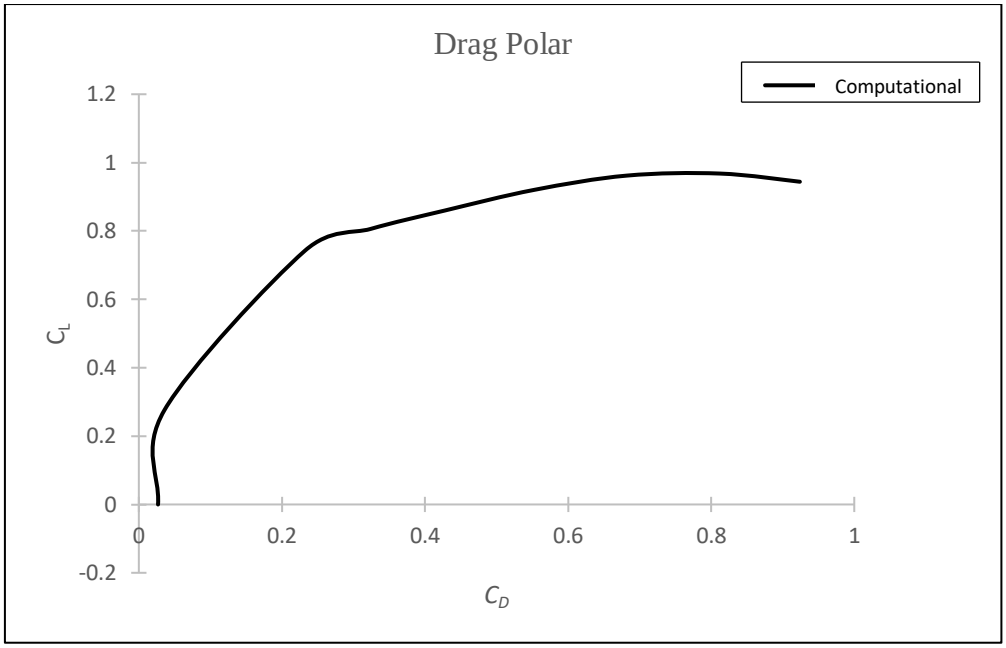


**Figure 4. 10:** Drag Polar for the BWB model ($U_\infty$=20m/s, Re=2.1x$10^5$)

### 4.2.2 Pressure Coefficient

From Figure 4.11 to Figure 16 shows the negative pressure coefficients(-Cp) values were plotted at the specified spanwise locations: 0.1 y/(b/2), 0.5 y/(b/2), 0.7 y/(b/2), and 0.9 y/(b/2) for the BWB model for various angles of attack. Figure 11 to Figure 16 also shows the pressure contours at each angle of attack. The discussion on Cp is performed for the upper surface only, as the main flow features are observed there.

#### 4.2.2.1 Pressure distribution at y/(b/2) = 0.1

Cp is measured at the 10% of the half span of the body. The aerofoil at this section is NACA 0017. For 0º angle of attack, since the aerofoil used is symmetrical aerofoil, Cp values for the upper and lower surface overlap over each other at all the locations. At low angles of attack, peak Cp value indicating decrease in pressure. As the angle of attack increases, the value of Cp also increases. Figure 4.11 shows the Cp distribution at 0º.

At angle of attack 20º, the pressure near the leading edge is very low than the ambient pressure and then gradually increases as we move downstream of the body such that at the trailing edge it is little higher than the ambient pressure. This indicates that the flow is still attached to the surface. Figure 4.12 shows the Cp distribution at 20º.

At angle of attack 30º, the pressure near the leading edge is lower than the ambient pressure and then gradually increases as we move downstream of the body till around 50% of the chord. Then Cp starts decreasing for some time and at the trailing edge it is almost equals the ambient pressure. Figure 4.13 shows the Cp distribution at 30º.

At angle of attack 40º, the pressure near the leading edge is lower than the ambient pressure and then gradually increases as we move downstream till around 40% of the chord. After this the Cp will decrease for some time and the becomes constant. This indicates that pressure is constant after x/c = 0.5, hence the flow separation has occurred. Figure 4.14 shows the Cp distribution at 40º.

At angle of attack 50º, the flow separation occurs at about 45% of the chord. The region of separated flow will have vortical air which forms stirred up wake region. The flow is separated for most part of the body. Figure 4.15 shows the Cp distribution at 50º.

At angle of attack 60º, the flow is fully separated from the body. After the separation, the suction of the wing at the leading edge reduces, hence less lift is produced. The flow is vortical all over the body. Figure 4.16 shows the Cp distribution at 60º.

#### 4.2.2.2 Pressure distribution at y/(b/2) = 0.5

Cp is measured at the 50% of the half span of the body. The aerofoil at this section is NACA 0017.At angle of attack 20º, the Cp value is constant all over the body. The flow is separated at this section. Figure 4.12 shows the Cp distribution at 20º. After separation, the Cp value all over the separated region becomes constant and is lower than the ambient pressure. Beyond angle of attack 20º, the Cp distribution shows a similar trend. The flow is fully separated on the upper surface at this section but the body will produce lift because the flow over the center body will be attached till angle of attack 40º. The large separation has occurred at this section before 20º and the wing is stalled.

#### 4.2.2.3 Pressure distribution at y/(b/2) = 0.7

Cp is measured at the 70% of the half span of the body. The aerofoil at this section is NACA 0012. As mentioned earlier, beyond 20º angle of attack, the flow is fully separated at this wing region and the wing is stalled. This phenomenon can also

be inferred from the Cp distribution plots. At angle of attack 20º, the Cp value is very low at the leading edge and then a sudden increase is observed and after that it becomes flat. Beyond angle of attack 20º, the Cp distribution shows a similar trend.

#### 4.2.2.4 Pressure distribution at y/(b/2) = 0.9

Cp is measured at the 90% of the half span of the body. The aerofoil at this section is NACA 0012. The flow over the wing separates at a low angle of attack as compared to other sections. At angle of attack 20º, the Cp at the leading edge becomes very low and then suddenly increases till 25% of the chord and then becomes flat.

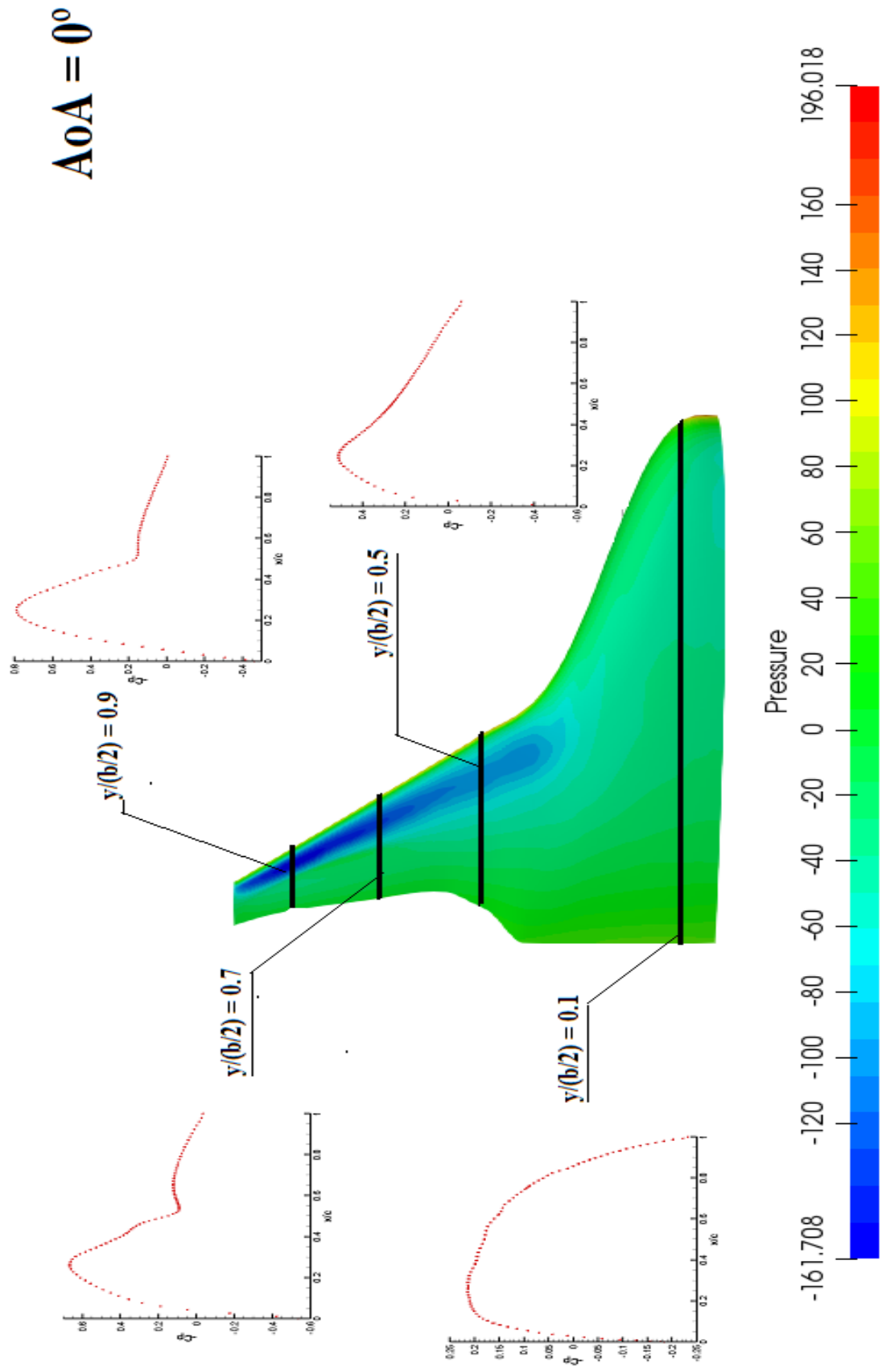


**Figure 4. 11:** Pressure distribution over the top surface of the BWB half model and Cp distribution at indicated spanwise locations at α=0º ($U_\infty$=20m/s, Re=2.1x$10^5$)

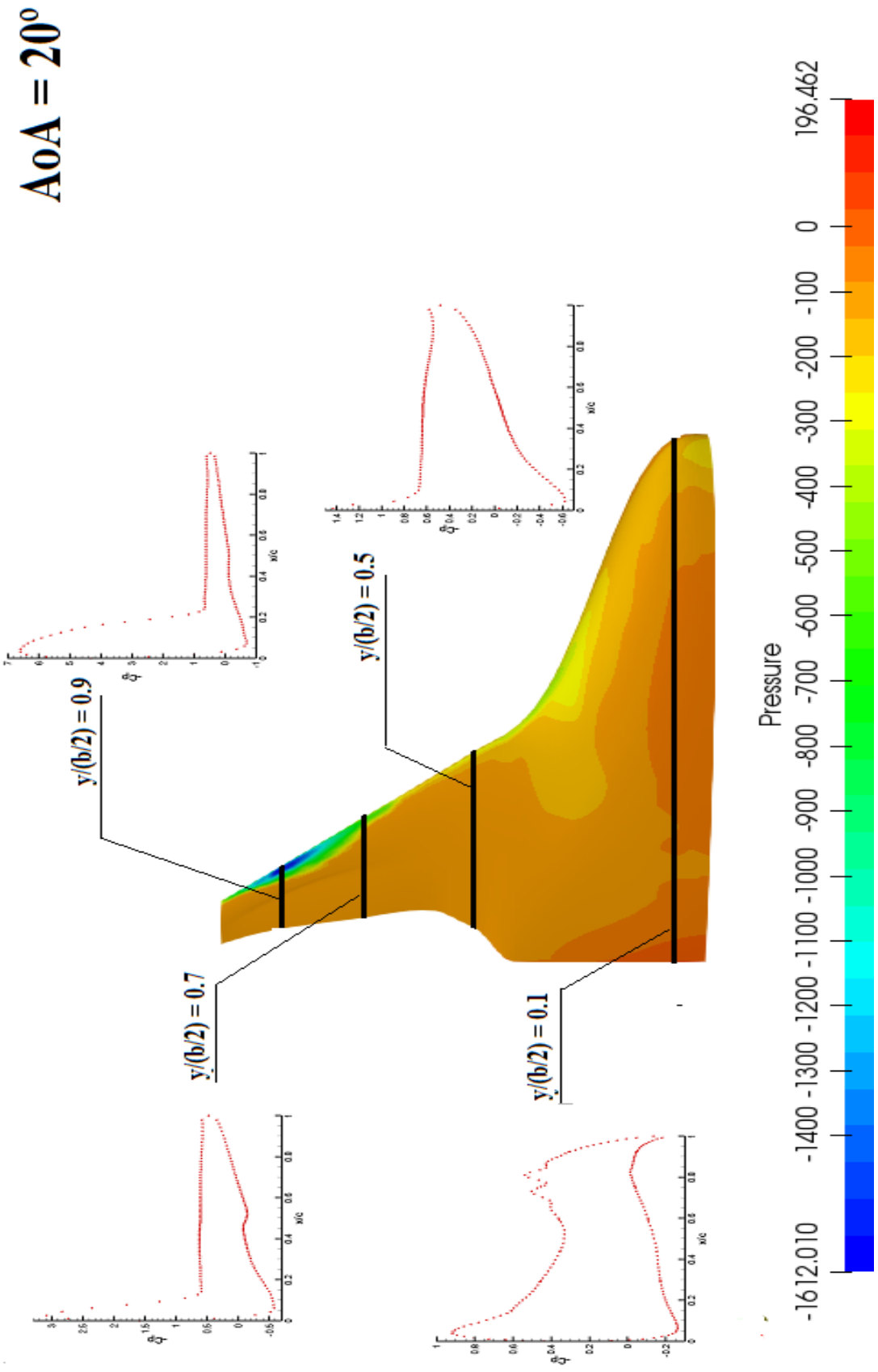


**Figure 4. 12:** Pressure distribution over the top surface of the BWB half model and Cp distribution at indicated spanwise locations at α=20º ($U_\infty$=20m/s, Re=2.1x$10^5$)

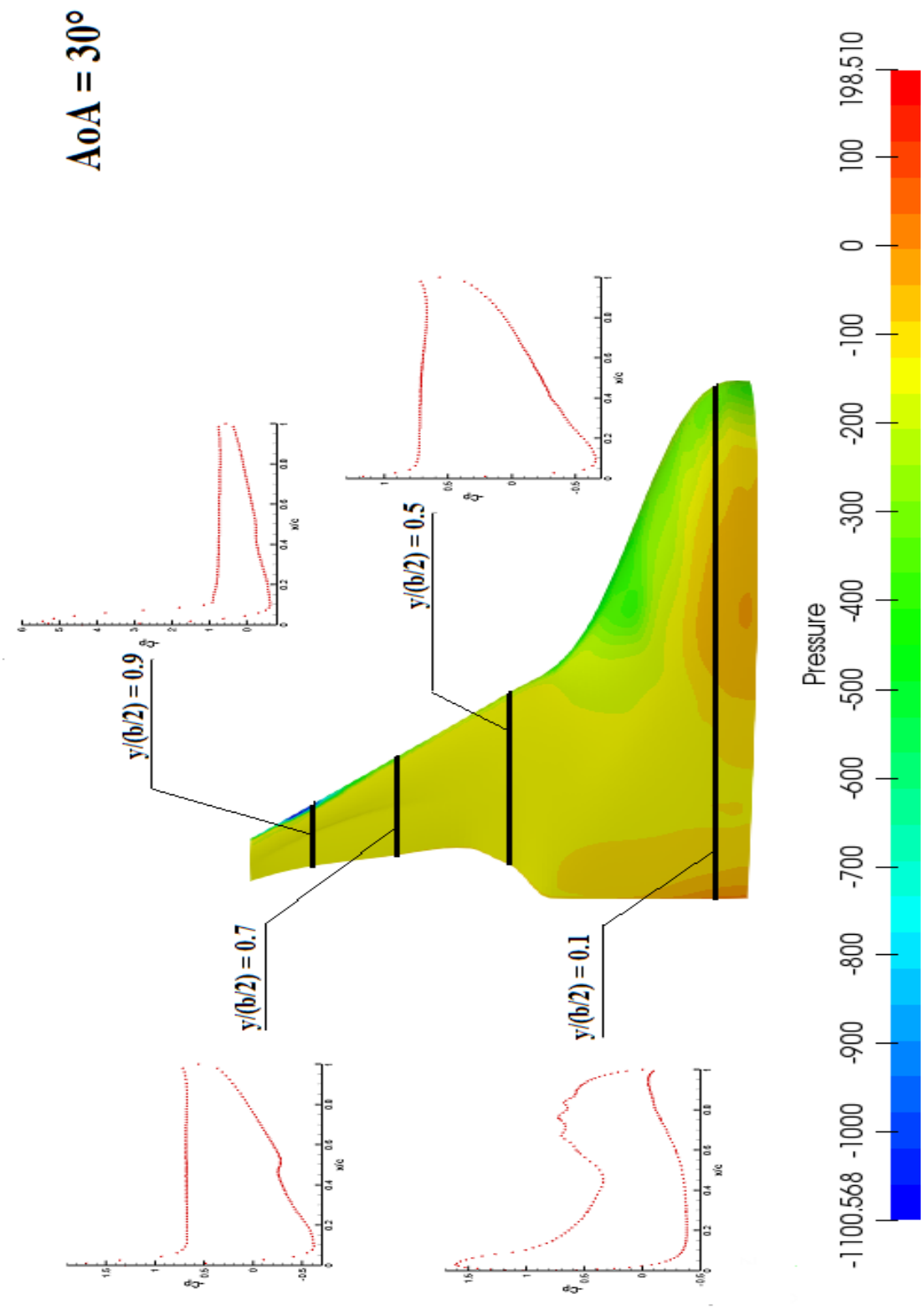


**Figure 4. 13:** Pressure distribution over the top surface of the BWB half model and Cp distribution at indicated spanwise locations at α=30º ($U_\infty$=20m/s, Re=2.1x$10^5$)

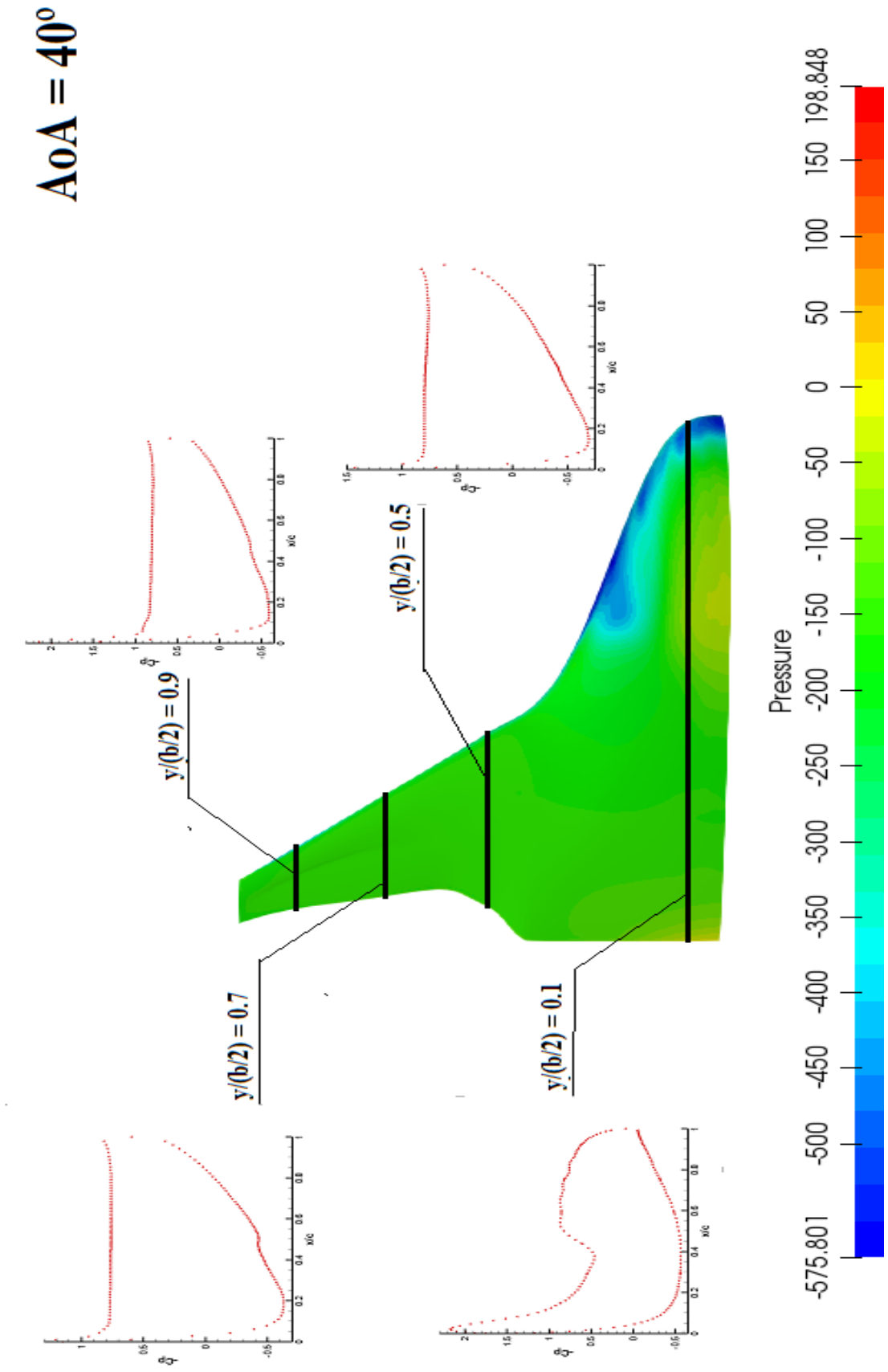


**Figure 4. 14:** Pressure distribution over the top surface of the BWB half model and Cp distribution at indicated spanwise locations at α=40º ($U_\infty$=20m/s, Re=2.1x$10^5$)

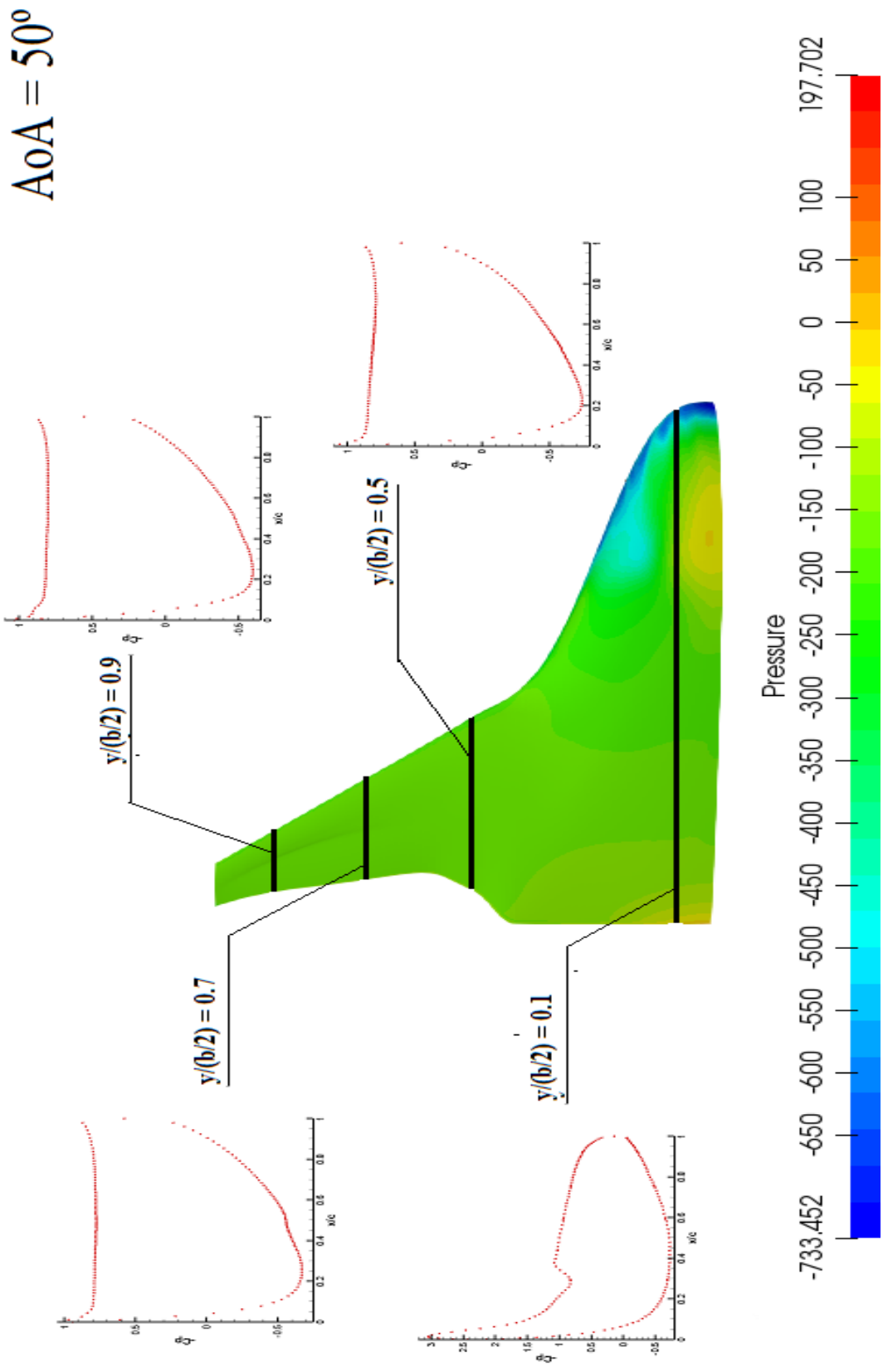


**Figure 4. 15:** Pressure distribution over the top surface of the BWB half model and Cp distribution at indicated spanwise locations at α=50º ($U_\infty$=20m/s, Re=2.1x$10^5$)

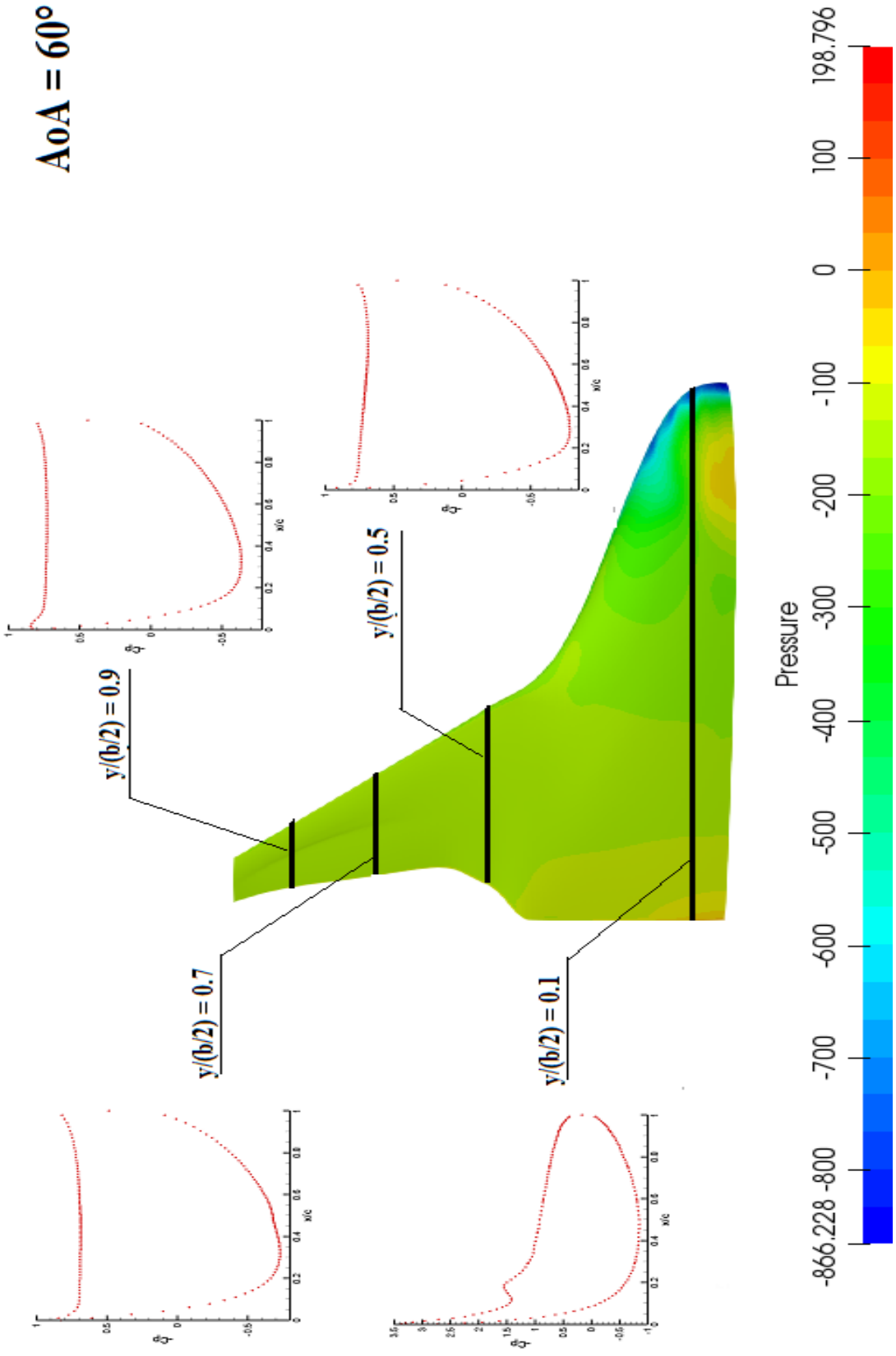


**Figure 4. 16:** Pressure distribution over the top surface of the BWB half model and Cp distribution at indicated spanwise locations at α=60º ($U_\infty$=20m/s, Re=2.1x$10^5$)

## 4.3 FLOW VISUALISATION

CFD analyses were carried out to simulate vortical flow over a 3-D BWB half model for a low subsonic speed.

### 4.3.1 Pathlines

The flow over the BWB model changes with the increase in the angle of attack. To visualise the flow behaviour over the BWB model, pathlines of the flow were created. Figure 14.17 show the pathlines over the model at different angle of attack.

At angle of attack 0º, the flow over the model leaves smoothly. Since only symmetrical aerofoils are used, the flow is attached to the surface of the model and no lift is produced.

At angle of attack 20º, the flow has fully separated at the wing of the body and the wing is stalled. The flow downstream of the wing is vortical in nature. But at the fuselage part, the flow is still fully attached to the body. Hence the body continues to produce lift even when the wing is stalled.

At angle of attack 30º, the flow starts separating at the downstream of the body and the vortices starts building up. The flow is fully attached at the center of the fuselage. When moving from the leading edge to trailing edge, the flow is attached till around 60% of the root chord.

At angle of attack 40º, the flow has fully separated near the trailing edge of the body, the circulation region has grown. The circulation region extends from x/c= 0.4 to the trailing edge. At the leading edge, the flow is still attached till around 40% of the root chord.

Beyond 40º, the flow will separate all over the body. the vortex starts lifting off the body in the circulation zone. The flow will be vortical over the surface of the

body and the whole body is also stalled. The lift is reduced after this angle of attack.

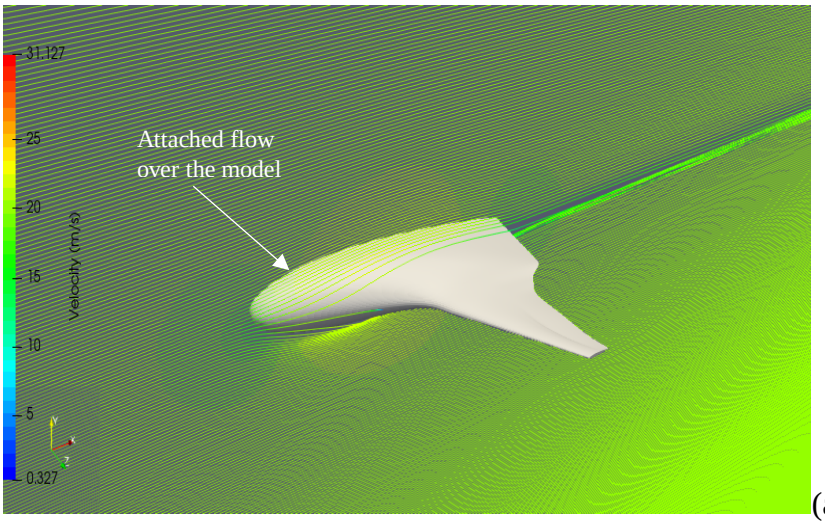


(a) AoA = 0º

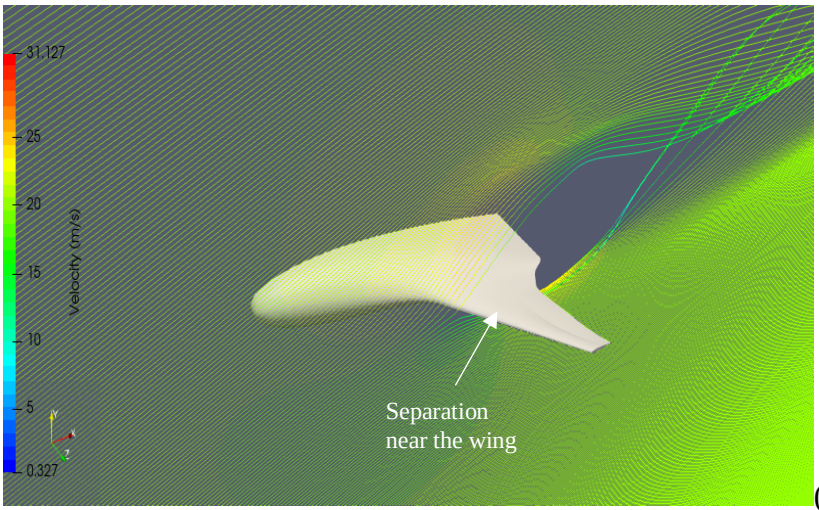


(b) AoA = 20º

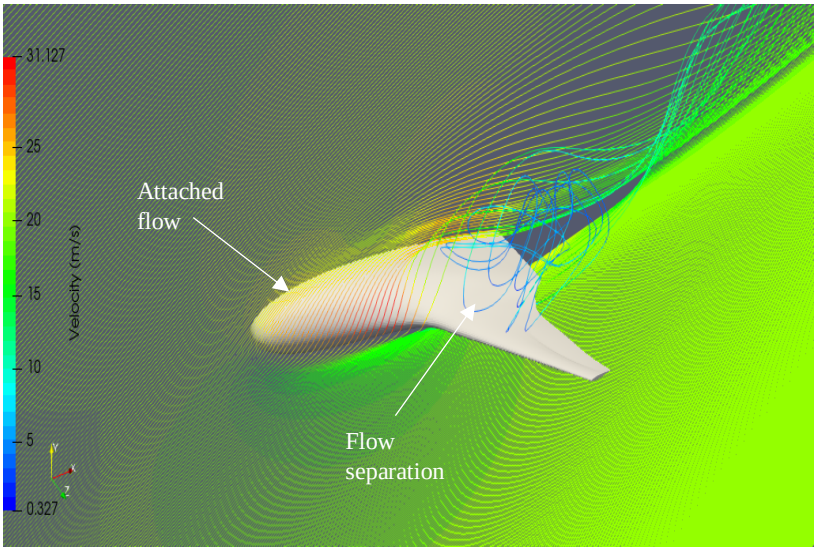


(b) AoA = 30º

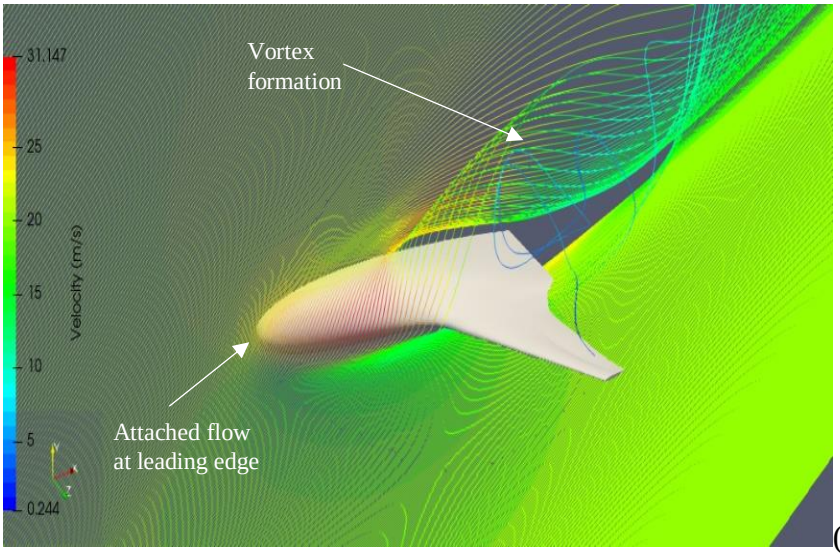


(b) AoA = 40º

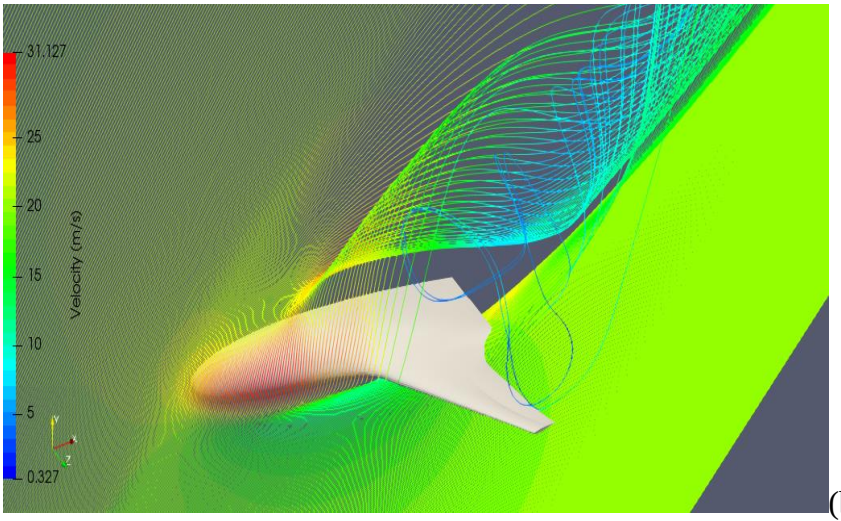


(b) AoA = 50º

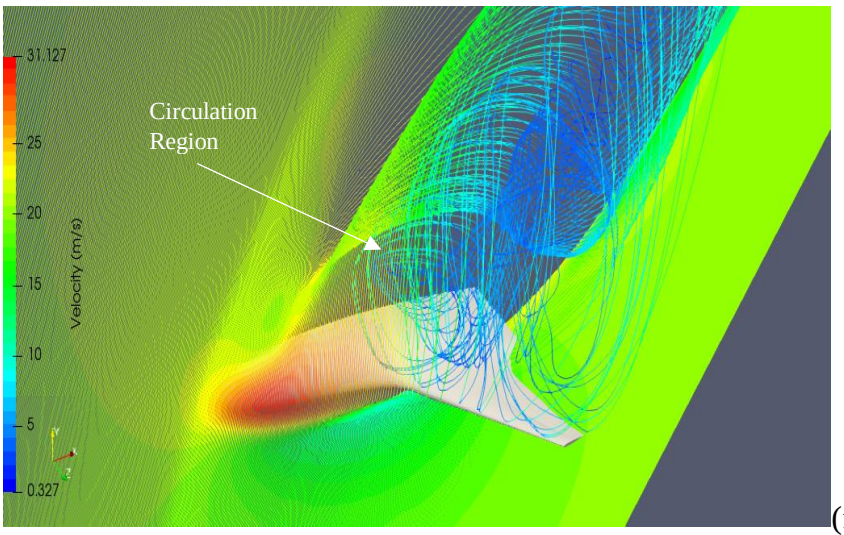


(f) AoA = 60º

**Figure 4. 17:** Pathlines over the BWB model at different angle of attack ($U_\infty$=20m/s, Re=2.1x$10^5$)

### 4.3.2 Streamlines

**S**treamlines were visualised on the upper surface of the BWB model to get a better understanding of the flow over the model at different angles of attack. Figure 4.18 shows the surface limiting streamlines over the BWB model at different angles of attack.

At angle of attack 0º, the streamlines are straight and is attached to the body. With the increase in the angle of attack, flow starts to separate. As the wing sectional profile is NACA 0012, around 12-15º, the flow separates at leading edge of wing, which leads to the stalling of the wing. At angle of attack 20º, the streamlines near the leading edge shows that separation has occurred. Small circulation region also begins over the wing.

At angle of attack 30º, the circulation in the region is increased, indicating that vortex is becoming strong. At the starting of the leading edge, the streamlines move parallel with the surface. To the downstream of the body, the flow becomes more vortical near the trailing edge.

Increasing the angle of attack, the vortices are spreading up and the strength of the vortex increases. The vortex structure moves upstream with the increasing angle of attack. These can be observed from the streamlines shown in Figure 4.18.

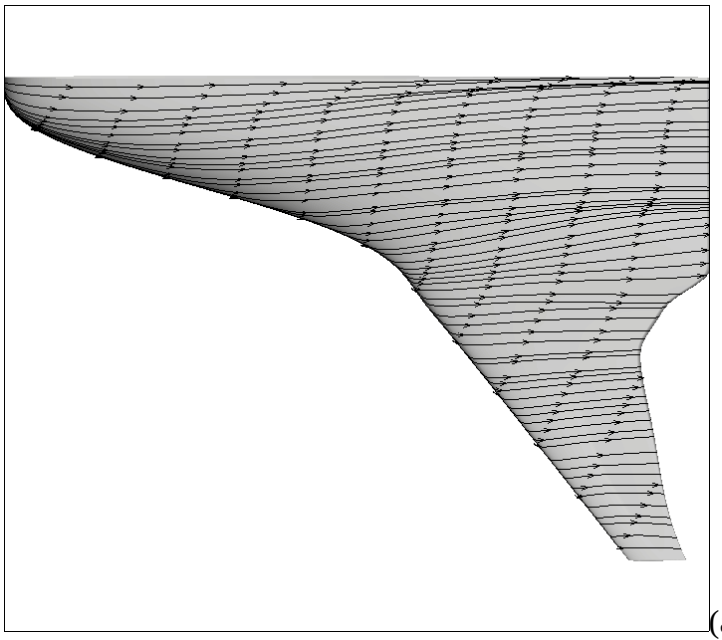

(a) AoA = 0º

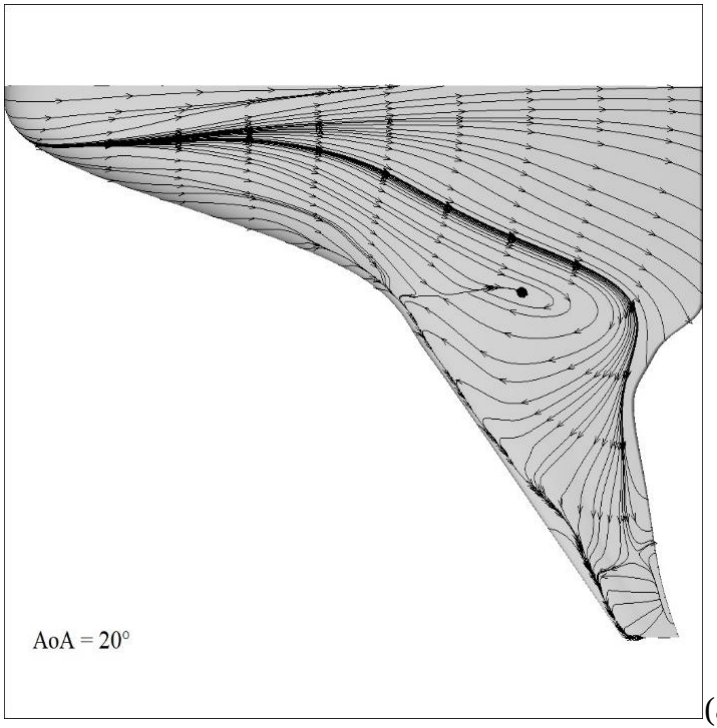

(a) AoA = 20º

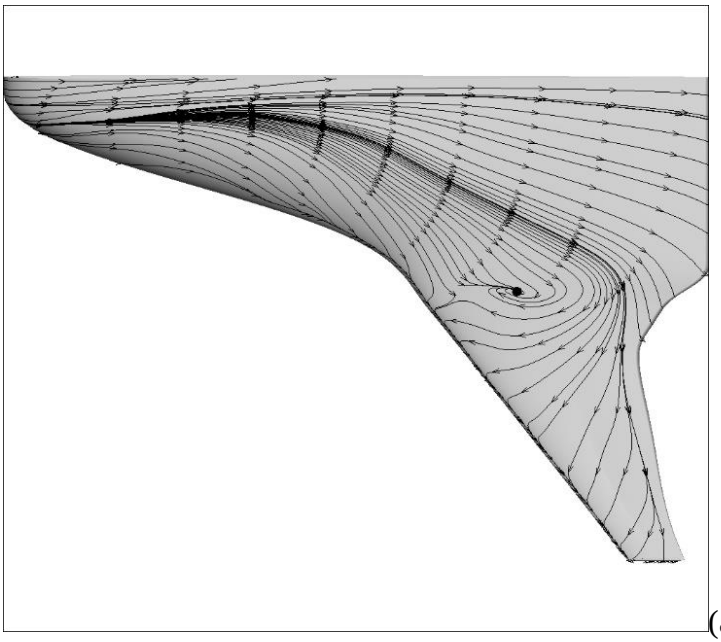
(a) AoA = 30º

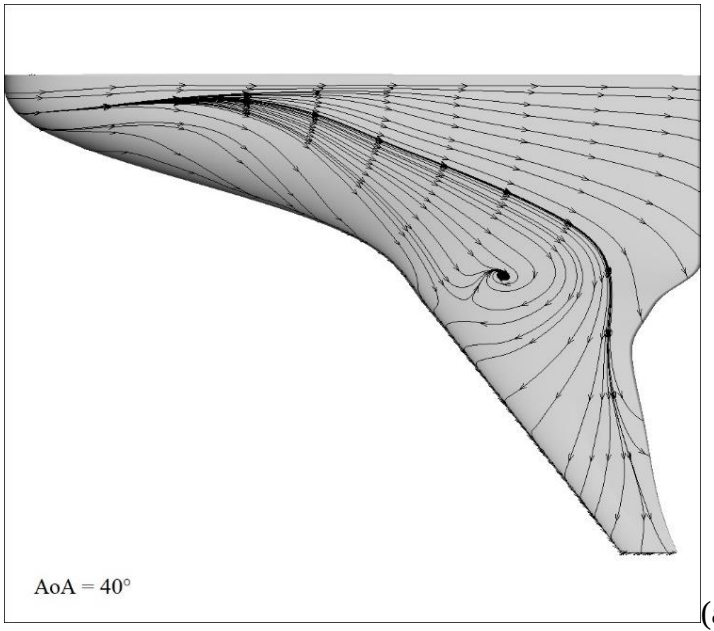

(a) AoA = 40º

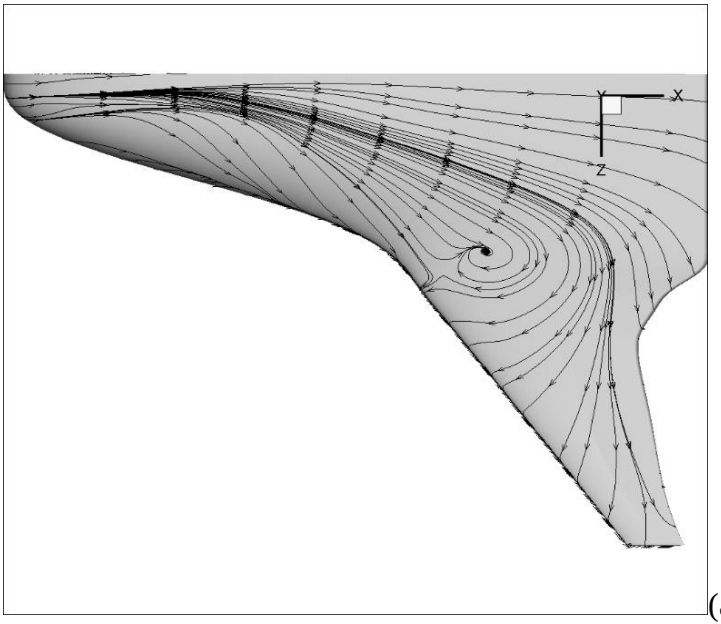

(a) AoA = 50º

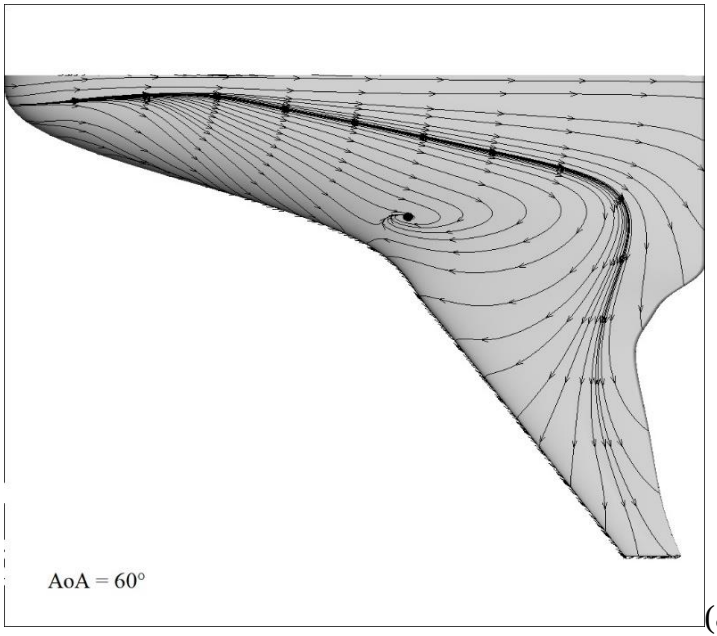


(a) AoA = 60º

**Figure 4. 18:** Streamline over the BWB model ($U_\infty$=20m/s, Re=2.1x$10^5$)

## 4.4 WIND TUNNEL TESTING

Quantitative and qualitative analysis of the BWB model were carried out using low speed wind tunnel. All the experiments were made at a Reynolds number of 2.1x$10^5$ with a flow speed of 20m/s. The experimental data were compared with the computational data obtained over the BWB model using OpenFOAM.

### 4.4.1 Comparison of Aerodynamic Characteristics

Quantitative analysis includes the measurement of force coefficients acting on the BWB model using a 5-component strain gauge balance. The experimental force coefficients are then compared with computational data at the same Reynolds number.

Figure 4.19 shows the increasing lift coefficients with the angle of attack as expected. The experimental results are in good match with the computational results. At higher angles of attack, near stall region the computations predict a slightly lower value than the experimental values.

Figure 4.20 shows the comparison of the experimental drag coefficient to that of the computed drag coefficient. At low angles of attack, the experimental values compare well with the computed values. As the angle of attack increases, the deviation in the experimental value and computational value also increases but the trend followed is same. The deviation in the values is because at higher angle of attack, there will be

large separated region over the body and turbulence model will not be effective to capture the flow physics properly.

Figure 4.21 shows the comparison of the L/D ratio obtained from the experiments and the computational value and Figure 4.22 shows the comparison of Drag Polar obtain from the experiment to that of the computational result. Both the graphs are in close agreement with each other.

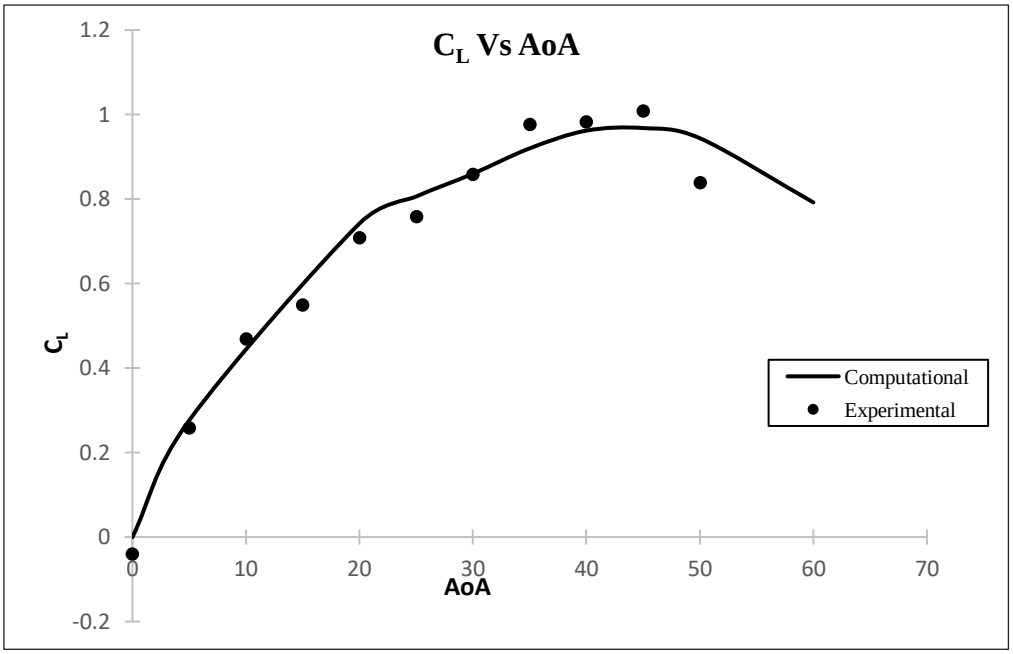


**Figure 4. 19:** Comparison of experimental and computational $C_L$ ($U_\infty$=20m/s, Re=2.1x$10^5$)

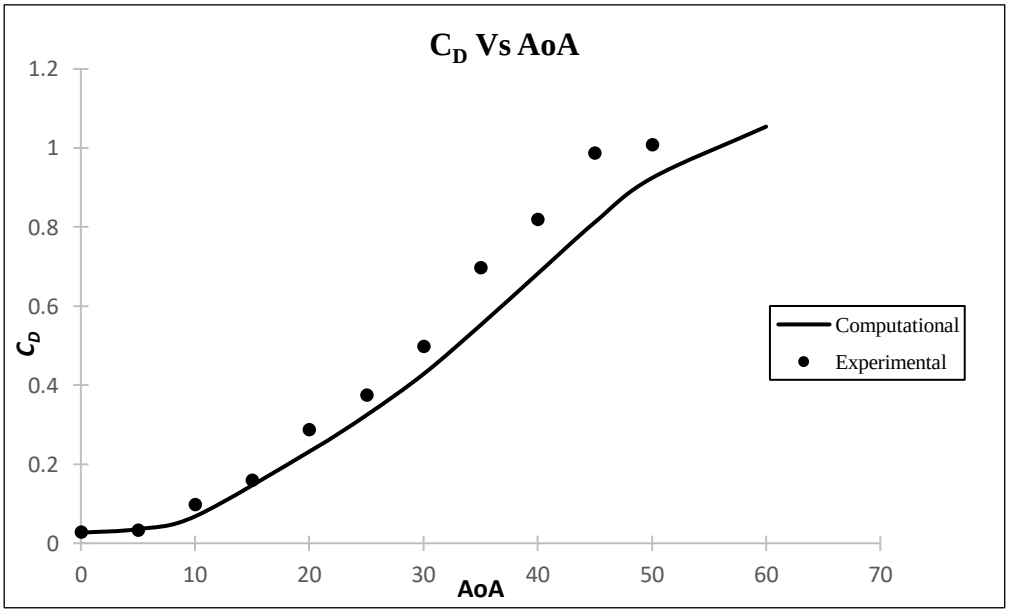


**Figure 4. 20:** Comparison of experimental and computational $C_D$

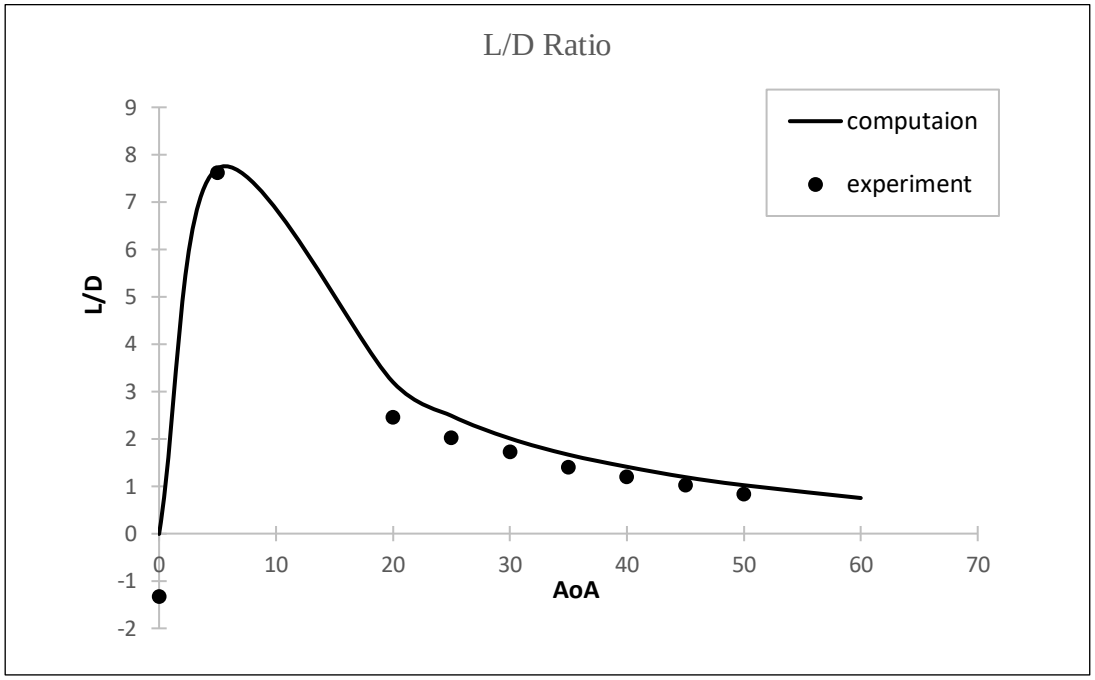


**Figure 4. 21:** Comparison of experimental and computational L/D Ratio ($U_\infty$=20m/s, Re=2.1x$10^5$)

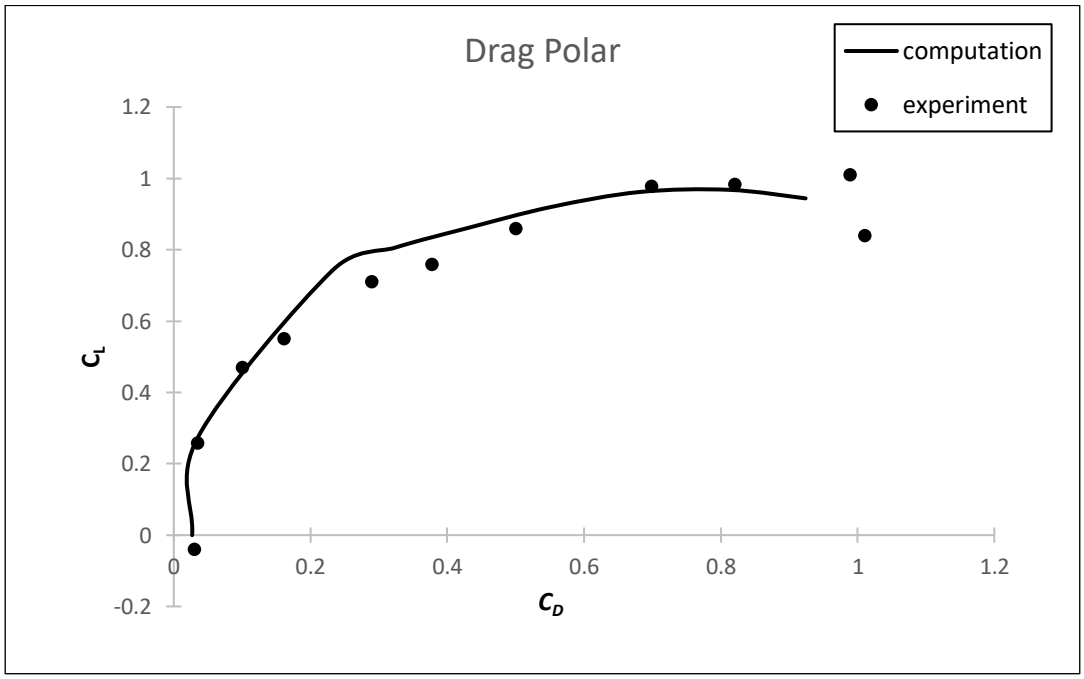


**Figure 4. 22:** Comparison of experimental and computational Drag Polar ($U_\infty$=20m/s, Re=2.1x$10^5$)

### 4.4.2 Tuft Flow Visualisation

Tuft flow visualisation technique is used to study the flow over the model. Tufts will align itself accordingly as air flows over the model. The tuft flow visualisation was carried out from 0º to 50º AoA. Figure 3 shows the tuft flow at major angles of attack.

At angle of attack 0º, the tufts are arranged in the direction of the flow all over the model. The flow is attached to the surface. At angle of attack 15º, the flow is separated at the wings. This is indicated by the reverse tufts' direction on the wing. As the angle of attack increases, the flow separation starts occurring at the downstream of the model.

At angle of attack 30º, the tufts are oscillating over the wing region but the at the leading edge of the center body, the tufts are aligned in downward direction. The vortical flow has occurred at the downstream of the model. At angle of attack 50 deg., the tufts all over the model are oscillating, indicating that the flow is fully separated from the model.

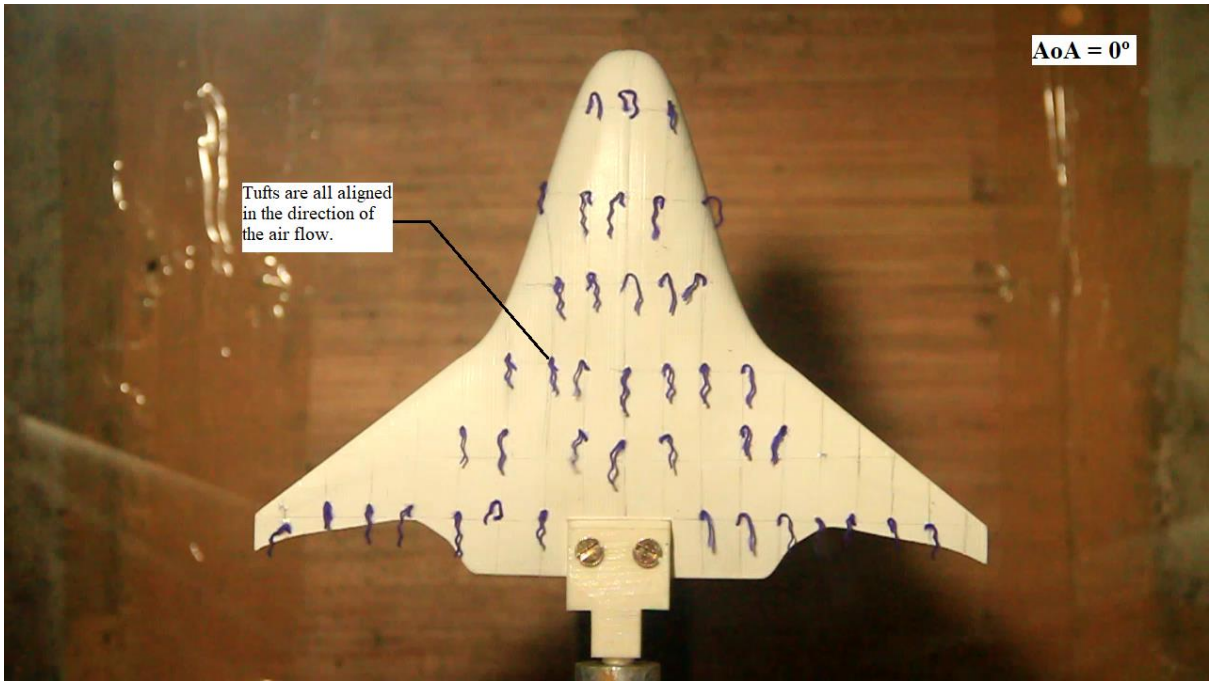


(a) AoA = 0º

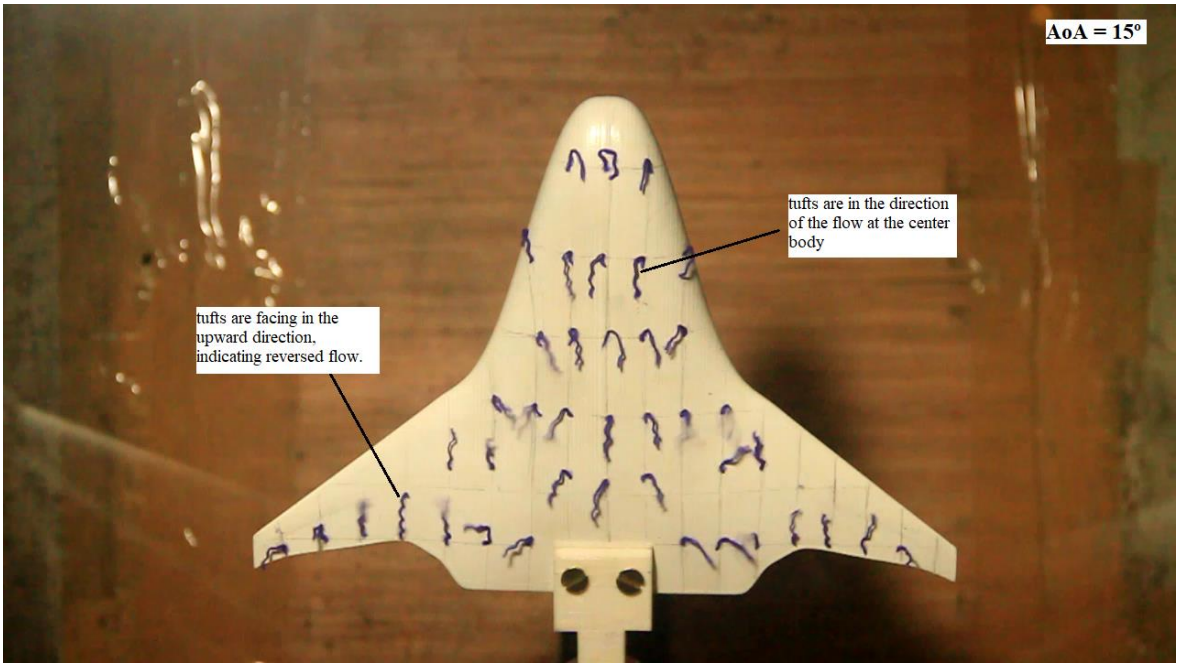


(b) AoA = 15º

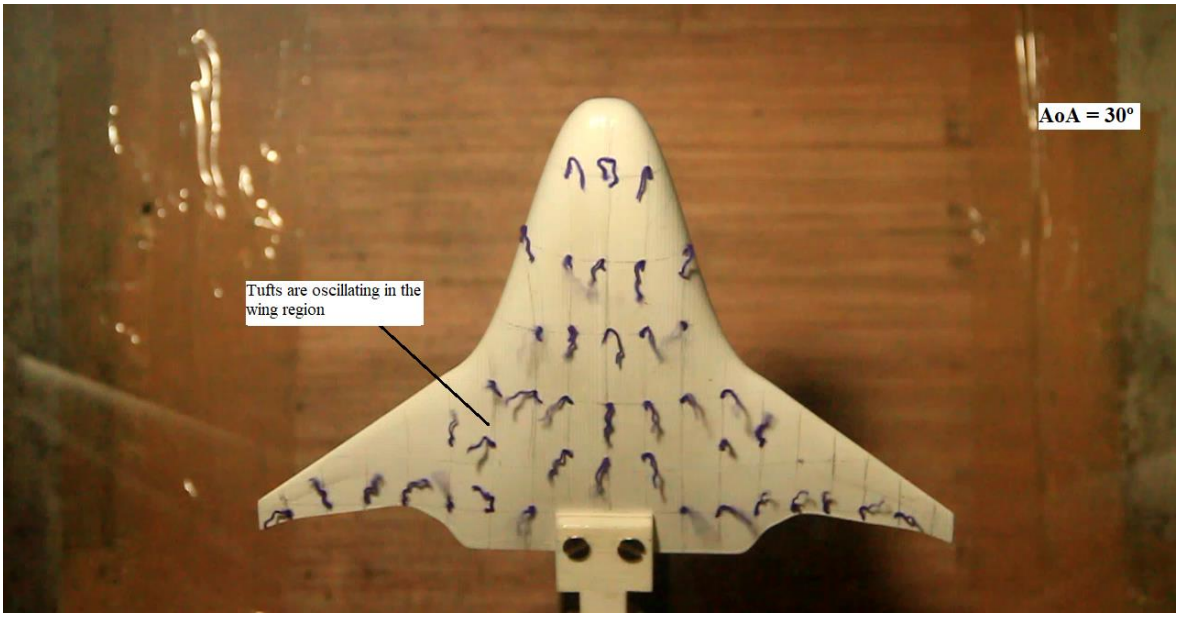


(c) AoA = 30º

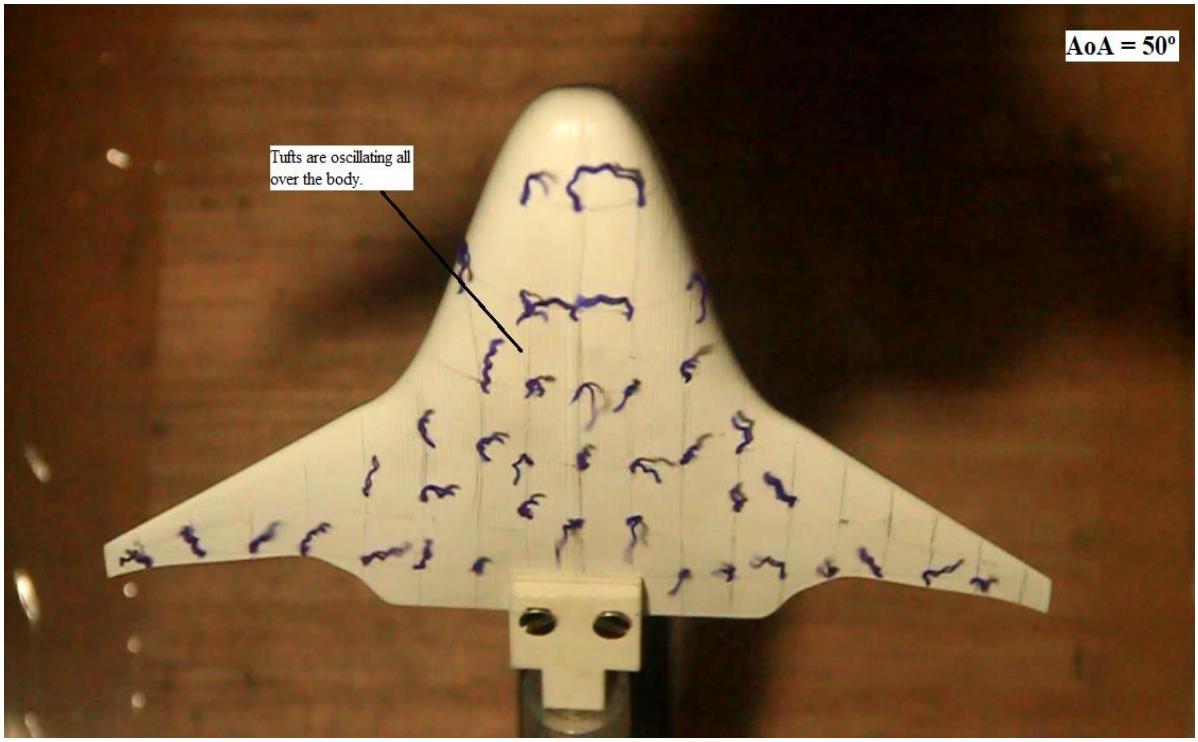


(d) AoA = 50º

**Figure 4. 23:** Tuft Flow Visualisation at different angle of attack ($U_\infty$=20m/s, Re=2.1x$10^5$)

# CHAPTER 5

# CONCLUSION

In the present investigation, numerical and experimental study have been done to understand the complex flow field over a Blended wing body. A 3-D BWB model designed in SoildWorks is used for the numerical investigations followed by wind tunnel experiments. CFD analysis is done on half model using OpenFOAM software while experimental analysis is done on a full model. Aerodynamic characteristics and flow features obtained from the CFD analysis have been studied, analysed and compared with the experimental results. All the analysis has been carried out at velocity 20m/s and Reynolds number $2.1 \times 10^5$.

Some important conclusions drawn from the current project are given below:

- The $C_L$ plot obtained from both CFD and experiment shows that the BWB configuration can fly at very high angle of attack (around $\alpha = 45^o$) before experiencing stall.
- For this configuration, the maximum L/D ratio is achieved at $\alpha = 6^o$. This is the optimal AoA for cruising of the BWB model.
- Flow separates over the wing at low angle of attack but remains attached over the center body.
- The wings have stalled at low angle of attack but the body will still produce lift with increasing angle of attack. Hence, the aircraft body is the main contributor of lift at high AoA.
- Vortices are observed over the body at AoA around $30^o$. Then, the circulation region will move upstream with the increase in the angle of attack.
- The strength of the vortices increases with the increase in angle of attack.
- The whole BWB body experience stall at $\alpha$ around $45^o$.

- The results from the CFD analysis shows that the BWB configuration exhibit satisfactory aerodynamic characteristics at low subsonic region. There is a close agreement of the numerical and experimental data.

In general, this project has been a satisfactory and was interesting experience analysing an unconventional aircraft like the Blended Wing Body with OpenFOAM software and wind tunnel experiments.

# CHAPTER 6

# SCOPE OF FUTURE WORK

Further studies which can be carried in this field of research are mentioned below:

- Flow visualisation using laser sheet can give a better understanding of the flow over the model.
- Analysis of BWB model in other fields such as aeroelasticity or aeroacoustics would be helpful.
- Optimisation techniques can be carried to optimise the model which will further improve the aerodynamic characteristics.
- Analysis can be carried out with different aerofoil profiles.
- LES and DES approaches can be used to capture more accurate aerodynamic performance. Better computational capabilities would be required to achieve it.
- Stability analysis can be performed over the model to study its static and dynamic stability.
- Further analysis can be done to study the effect of yaw, roll, Mach number etc.

# REFERENCES


[1] R. H. Liebeck, M. A. Potsdam, M. A. Page, "Blended wing body Analysis and Design", AIAA-97-2317, 1997.

[2] R. H. Liebeck, M. A. Page, B. K. Rawdon, "Blended-wing-body subsonic commercial transport", 36th Aerospace Science Meeting and Exhibit, AIAA-98-0438, 1998.

[3] R. H. Liebeck, "Blended wing body design challenges", International Air and Space Symposium and Exposition, AIAA 2003-2659, 2003.

[4] R. H. Liebeck, "Design of the blended wing body subsonic transport", Journal of Aircraft, Vol. 41, pp. 10–25, 2004.

[5] P. Dehpanah and A. Nejat, "The Aerodynamic Design Evaluation of a Blended-Wing-Body Configuration", Aerospace Science and Technology, Vol. 43, pp. 96–110, 2015.

[6] Zurriati Mohd Ali, W. Kuntjoro, W. Wisnoe, Rizal Effendy Mohd Nasir and N.I. Ismail, "Numerical Study of Aerodynamic Characteristics on Blended Wing Body Aircraft with Small Canard", Pertanika Journal of Science & Technology, Vol. 25, pp. 9–18, 2017.

[7] N. Qin, A. Vavalle, A. Le Moigne, M. Laban, K. Hackett, P. Weinerfelt, "Aerodynamic Considerations of Blended Wing Body Aircraft", Progress in Aerospace Sciences, Vol. 40, pp. 321–343, 2004.

[8] Roberto Merino-Martinez, "Design and Analysis of the Control and Stability of a Blended Wing Body Aircraft", MSc. Thesis, Royal Institute of Technology (KTH), 2015.

[9] D Roman, R. Gilmore, S. Wakayama, "Aerodynamics of High Subsonic Blended-Wing-Body Configurations", 41st Aerospace Sciences Meeting and Exhibit, AIAA Paper 2003-554, 2003.

[10] Z. Lyu and Joaquim R. R. A. Martins, "RANS-based Aerodynamic Shape Optimization of a Blended-Wing-Body Aircraft", 21st AIAA Computational Fluid Dynamics Conference, AIAA 2013-2586, 2013.

[11] Paul Okonkwo, “Conceptual Design Methodology for Blended Wing Body Aircraft”, PhD Thesis, Cranfield University, 2016.

[12] Paul Okonkwo and Howard Smith, “Review of evolving trends in blended wing body aircraft design”, Progress in Aerospace Sciences, Vol. 82, pp. 1–23, 2016.

[13] N. B. Kuntawala, “Aerodynamic Shape Optimization of a Blended-Wing-Body Aircraft Configuration”, Master's thesis, University of Toronto, 2011.

[14] N. B. Kuntawala, J. E. Hicken, and D. W. Zingg, “Preliminary Aerodynamic Shape Optimization of a Blended-Wing-Body Aircraft Configuration”, 49th AIAA Aerospace Sciences Meeting including the New Horizons Forum and Aerospace Exposition, AIAA 2011-642, 2011.

[15] T. Ikeda, “Aerodynamic Analysis of a Blended-Wing-Body Aircraft Configuration”, Master Thesis, RMIT University, 2006.

[16] Richard J. Re, “Longitudinal Aerodynamic Characteristics and Wing Pressure Distributions of a Blended Wing Body Configuration at Low and High Reynolds Numbers”, NASA/TM-2005-213754, 2005.

[17] D. J. Thompson, J. Feys, M. D. Filewich, Sharif Abdel-Magid, D. Dalli, and F. Goto, “The Design and Construction of a Blended Wing Body UAV”, 49th AIAA Aerospace Sciences Meeting including the New Horizons Forum and Aerospace Exposition, AIAA 2011-841, 2011.

[18] Sami Ammar, Clément Legros, Jean-Yves Trépanier, “Conceptual design, performance and stability analysis of a 200 passengers Blended Wing Body aircraft”, Aerospace Science and Technology, Vol. 71, pp. 325–336, 2017.

[19] Baig AZ, Cheema TA, Aslam Z, Khan YM, Sajid Dar H, “A New Methodology for Aerodynamic Design and Analysis of a Small-Scale Blended Wing Body”, Journal of Aeronautics and Aerospace Engineering, Vol. 7, 2018.

[20] Geoffrey Larkin and Graham Coates, “A design analysis of vertical stabilisers for Blended Wing Body aircraft”, Aerospace Science and Technology, Vol. 64, pp. 237-252, 2017.

[21] M. Zhang, A. Rizzi, P. Meng, R. Nangia, R. Amiree, O. Amoignon, “Aerodynamic Design Considerations and Shape Optimization of Flying Wings in Transonic Flight”, 12th AIAA Aviation Technology, Integration, and Operations (ATIO) Conference, AIAA 2012-5402, 2012.

[22] P. R. Spalart and S. R. Allmaras, “A One-Equation Turbulence Model for Aerodynamic Flows”, AIAA 1992-0439, 1992.

[23] Martin Carlsson and Jakob Kuttenkeuler, “Design and Testing of a Blended Wing Body Aeroelastic Wind-Tunnel Model”, Journal of Aircraft, Vol. 40, 2002.

[24] D. J Triton, “Experiments on the Flow Past a Circular Cylinder at Low Reynolds Number”, JFM, Vol. 6, pp. 547-567, 1959.

[25] P. H. Cook, M. A. Mc Donald, M.C.P Firmin, “Aerofoil RAE 2822-Pressure distribution and Boundary Layer and wake measurement”, AGARD AR-138, 1979.

[26] OpenFOAM® - Official home of The Open Source Computational Fluid Dynamics (CFD) Toolbox: *http://www.openfoam.com/* (accessed April 2019).

[27] Pitch and Yaw mechanism: *http://halmarc.com/pitch_&_yaw_&_mechanism.php*

[28] NACA 4-digit airfoil generator: *http://airfoiltools.com/airfoil/naca4digit/* (accessed April 2019).

# Appendix

## A: OpenFOAM case files for BWB model at AoA 30º

### File: *p*

```
/*--------------------------------*- C++ -*----------------------------------*\
| =========                 |                                                 |
| \\      /  F ield         | OpenFOAM: The Open Source CFD Toolbox           |
|  \\    /   O peration     | Version:  5.x                                   |
|   \\  /    A nd           | Web:      www.OpenFOAM.org                      |
|    \\/     M anipulation  |                                                 |
\*---------------------------------------------------------------------------*/
FoamFile
{
    version     2.0;
    format      ascii;
    class       volScalarField;
    location    "0";
    object      p;
}
// * * * * * * * * * * * * * * * * * * * * * * * * * * * * * * * * * * * * * * * * //
dimensions      [0 2 -2 0 0 0 0];

internalField   uniform 0;

boundaryField
{
    side
    {
        type            zeroGradient;
    }
    symmetry
    {
        type            symmetry;
    }
    inlet
    {
        type            zeroGradient;
    }
    outlet
    {
        type            fixedValue;
        value           uniform 0;
    }
    bottom
    {
        type            zeroGradient;
    }
    top
    {
        type            zeroGradient;
    }
    bwb
    {
        type            zeroGradient;
    }
}
// ************************************************************************* //
```

**File: *U***

```
/*--------------------------------*- C++ -*----------------------------------*\
| =========                 |                                                 |
| \\      /  F ield         | OpenFOAM: The Open Source CFD Toolbox           |
|  \\    /   O peration     | Version:  5.x                                   |
|   \\  /    A nd           | Web:      www.OpenFOAM.org                      |
|    \\/     M anipulation  |                                                 |
\*---------------------------------------------------------------------------*/
FoamFile
{
    version     2.0;
    format      ascii;
    class       volVectorField;
    location    "0";
    object      U;
}
// * * * * * * * * * * * * * * * * * * * * * * * * * * * * * * * * * * * * * * * //
dimensions      [0 1 -1 0 0 0 0];

internalField   uniform (17.3205 10 0);

boundaryField
{
    side
    {
        type            zeroGradient;
    }
    symmetry
    {
        type            symmetry;
    }
    inlet
    {
        type            fixedValue;
        value           uniform (17.3205 10 0);
    }
    outlet
    {
        type            zeroGradient;
    }
    bottom
    {
        type            zeroGradient;
    }
    top
    {
        type            zeroGradient;
    }
    bwb
    {
        type            fixedValue;
        value           uniform (0 0 0);
    }
}
// ************************************************************************* //
```

**File: *nuTilda***

```
/*--------------------------------*- C++ -*----------------------------------*\
| =========                 |                                                 |
| \\      /  F ield         | OpenFOAM: The Open Source CFD Toolbox           |
|  \\    /   O peration     | Version:  5.x                                   |
|   \\  /    A nd           | Web:      www.OpenFOAM.org                      |
|    \\/     M anipulation  |                                                 |
\*---------------------------------------------------------------------------*/
FoamFile
{
    version     2.0;
    format      ascii;
    class       volScalarField;
    location    "0";
    object      nuTilda;
}
// * * * * * * * * * * * * * * * * * * * * * * * * * * * * * * * * * * * * * * * //
dimensions      [0 2 -1 0 0 0 0];

internalField   uniform 4.3812e-05;

boundaryField
{
    side
    {
        type            zeroGradient;
    }
    symmetry
    {
        type            symmetry;
    }
    inlet
    {
        type            fixedValue;
        value           uniform 4.3812e-05;
    }
    outlet
    {
        type            zeroGradient;
    }
    bottom
    {
        type            zeroGradient;
    }
    top
    {
        type            zeroGradient;
    }
    bwb
    {
        type            fixedValue;
        value           uniform 0;
    }
}
// ************************************************************************* //
```

**File: *nut***

```
/*--------------------------------*- C++ -*----------------------------------*\
| =========                 |                                                 |
| \\      /  F ield         | OpenFOAM: The Open Source CFD Toolbox           |
|  \\    /   O peration     | Version:  5.x                                   |
|   \\  /    A nd           | Web:      www.OpenFOAM.org                      |
|    \\/     M anipulation  |                                                 |
\*---------------------------------------------------------------------------*/
FoamFile
{
    version     2.0;
    format      ascii;
    class       volScalarField;
    location    "0";
    object      nut;
}
// * * * * * * * * * * * * * * * * * * * * * * * * * * * * * * * * * * * * * * * //
dimensions      [0 2 -1 0 0 0 0];

internalField   uniform 3.0712e-06;

boundaryField
{
    side
    {
        type            zeroGradient;
    }
    symmetry
    {
        type            symmetry;
    }
    inlet
    {
        type            fixedValue;
        value           uniform 3.0712e-06;
    }
    outlet
    {
        type            zeroGradient;
    }
    bottom
    {
        type            zeroGradient;
    }
    top
    {
        type            zeroGradient;
    }
    bwb
    {
        type            nutUSpaldingWallFunction;
        value           uniform 3.0712e-06;
    }
}
// ************************************************************************* //
```

**File: *transportProperties***

```
/*--------------------------------*- C++ -*----------------------------------*\
| =========                 |                                                 |
| \\      /  F ield         | OpenFOAM: The Open Source CFD Toolbox           |
|  \\    /   O peration     | Version:  5                                     |
|   \\  /    A nd           | Web:      www.OpenFOAM.org                      |
|    \\/     M anipulation  |                                                 |
\*---------------------------------------------------------------------------*/
FoamFile
{
    version     2.0;
    format      ascii;
    class       dictionary;
    location    "constant";
    object      transportProperties;
}
// * * * * * * * * * * * * * * * * * * * * * * * * * * * * * * * * * * * * * //
transportModel  Newtonian;

rho             [1 -3 0 0 0 0 0] 1.225;
nu              [0 2 -1 0 0 0 0] 1.4604e-05;
// ************************************************************************* //
```

**File: *turbulenceProperties***

```
/*--------------------------------*- C++ -*----------------------------------*\
| =========                 |                                                 |
| \\      /  F ield         | OpenFOAM: The Open Source CFD Toolbox           |
|  \\    /   O peration     | Version:  5                                     |
|   \\  /    A nd           | Web:      www.OpenFOAM.org                      |
|    \\/     M anipulation  |                                                 |
\*---------------------------------------------------------------------------*/
FoamFile
{
    version     2.0;
    format      ascii;
    class       dictionary;
    location    "constant";
    object      turbulenceProperties;
}
// * * * * * * * * * * * * * * * * * * * * * * * * * * * * * * * * * * * * * //
simulationType RAS;

RAS
{
    RASModel        SpalartAllmaras;
    turbulence      on;
    printCoeffs     on;
}
// ************************************************************************* //
```

**File: *controlDict***

```
/*--------------------------------*- C++ -*----------------------------------*\
| =========                 |                                                 |
| \\      /  F ield         | OpenFOAM: The Open Source CFD Toolbox           |
|  \\    /   O peration     | Version:  5                                     |
|   \\  /    A nd           | Web:      www.OpenFOAM.org                      |
|    \\/     M anipulation  |                                                 |
\*---------------------------------------------------------------------------*/
FoamFile
{
    version     2.0;
    format      ascii;
    class       dictionary;
    location    "system";
    object      controlDict;
}
// * * * * * * * * * * * * * * * * * * * * * * * * * * * * * * * * * * * * * //
application     simpleFoam;
startFrom       latestTime;
stopAt          endTime;
endTime         5000;
deltaT          1;
writeControl    timeStep;
writeInterval   50;
purgeWrite      30;
writeFormat     ascii;
writePrecision  6;
writeCompression off;
timeFormat      general;
timePrecision   6;
runTimeModifiable true;

functions
{
forces
     {
        type forces;
        libs ("libforces.so"); //Lib to load
        patches     (bwb);
        rhoInf 1.225; //Reference density for fluid
        rho   rhoInf;
        CofR (0.25 0 0); //Origin for moment calculations
        writeControl timeStep;
       timeInterval 1;
        log          true;
     }
forceCoeffs
     {
       type forceCoeffs;
       libs ("libforces.so");
       patches             (bwb);
       rhoInf 1.225;
       rho rhoInf;
      log       true;
       CofR (0.25 0 0);
        liftDir (-0.5 0.8660 0);
       dragDir (0.8660 0.5 0);
       pitchAxis (0 0 1);
       magUInf 20;
       lRef 0.15714;
       Aref 0.01454;
       writeControl timeStep;
       timeInterval 1;
     }
};
// ************************************************************************* //
```

**File: *decomposeParDict***

```
/*--------------------------------*- C++ -*----------------------------------*\
| =========                 |                                                 |
| \\      /  F ield         | OpenFOAM: The Open Source CFD Toolbox           |
|  \\    /   O peration     | Version:  5                                     |
|   \\  /    A nd           | Web:      www.OpenFOAM.org                      |
|    \\/     M anipulation  |                                                 |
\*---------------------------------------------------------------------------*/
FoamFile
{
    version     2.0;
    format      ascii;
    class       dictionary;
    location    "system";
    object      decomposeParDict;
}
// * * * * * * * * * * * * * * * * * * * * * * * * * * * * * * * * * * * * * //
numberOfSubdomains 4;
method          simple;
simpleCoeffs
{
    n               (2 2 1);
    delta           0.001;
}
hierarchicalCoeffs
{
    n               (1 1 1);
    delta           0.001;
    order           xyz;
}
manualCoeffs
{
    dataFile        "";
}
distributed     no;
roots           ( );
// ************************************************************************* //
```

**File: *fvSchemes***

```
/*--------------------------------*- C++ -*----------------------------------*\
| =========                 |                                                 |
| \\      /  F ield         | OpenFOAM: The Open Source CFD Toolbox           |
|  \\    /   O peration     | Version:  5                                     |
|   \\  /    A nd           | Web:      www.OpenFOAM.org                      |
|    \\/     M anipulation  |                                                 |
\*---------------------------------------------------------------------------*/
FoamFile
{
    version     2.0;
    format      ascii;
    class       dictionary;
    location    "system";
    object      fvSchemes;
}
// * * * * * * * * * * * * * * * * * * * * * * * * * * * * * * * * * * * * * * * //
ddtSchemes
{
    default         steadyState;
}
gradSchemes
{
      default cellLimited leastSquares 1.0;
      grad(U) cellLimited leastSquares 1.0;
}
divSchemes
{
    default         none;
    div(phi,U)       Gauss linearUpwind grad(U);
   div(phi,nuTilda)      Gauss upwind;
    div((nuEff*dev2(T(grad(U))))) Gauss linear;
}
laplacianSchemes
{
   default         Gauss linear limited 0.33;
}
interpolationSchemes
{
    default         linear;
}
snGradSchemes
{
   default         limited 0.33;
}
wallDist
{
    method meshWave;
}
// ************************************************************************* //
```

**File: *fvSolution***

```
/*--------------------------------*- C++ -*----------------------------------*\
| =========                 |                                                 |
| \\      /  F ield         | OpenFOAM: The Open Source CFD Toolbox           |
|  \\    /   O peration     | Version:  5                                     |
|   \\  /    A nd           | Web:      www.OpenFOAM.org                      |
|    \\/     M anipulation  |                                                 |
\*---------------------------------------------------------------------------*/
FoamFile
{
    version     2.0;
    format      ascii;
    class       dictionary;
    location    "system";
    object      fvSolution;
}
// * * * * * * * * * * * * * * * * * * * * * * * * * * * * * * * * * * * * * //
solvers
{
    p
    {
        solver          GAMG;
        tolerance       1e-05;
        relTol          0.01;
        smoother        GaussSeidel;
    }
    U
    {
        solver          smoothSolver;
        smoother        GaussSeidel;
        nSweeps         2;
        tolerance       1e-08;
        relTol          0.1;
    }
    nuTilda
    {
        solver          smoothSolver;
        smoother        GaussSeidel;
        nSweeps         2;
        tolerance       1e-08;
        relTol          0.1;
    }
}
SIMPLE
{
    nNonOrthogonalCorrectors 3;
    pRefCell        0;
    pRefValue       0;
    residualControl
    {
        p               1e-8;
        U               1e-8;
        nuTilda         1e-8;
    }
}
relaxationFactors
{
    fields
    {
        p               0.3;
    }
    equations
    {
        U               0.7;
        nuTilda         0.7;
    }
}
```